Fall 12-2020

Parametric Analysis of Particle Spreading with Discrete Element Method

Yuxuan Wu
Embry-Riddle Aeronautical University

PARAMETRIC ANALYSIS OF PARTICLE SPREADING WITH DISCRETE ELEMENT METHOD

By

Yuxuan Wu

A Thesis Submitted to the Faculty of Embry-Riddle Aeronautical University

In Partial Fulfillment of the Requirements for the Degree of

Master of Science in Aerospace Engineering

December 2020

Embry-Riddle Aeronautical University

Daytona Beach, Florida

PARAMETRIC ANALYSIS OF PARTICLE SPREADING WITH DISCRETE ELEMENT METHOD

By

Yuxuan Wu

This thesis was prepared under the direction of the candidate's Thesis Committee Chair, Dr. Sirish Namilae, Department of Aerospace Engineering, and has been approved by the members of the Thesis Committee. It was submitted to the office of the Senior Vice President for Academic Affairs and Provost, and was accepted in the partial fulfillment of the requirements for the Degree of Master of Science in Aerospace Engineering.

THESIS COMMITTEE

Chairman, Dr. Sirish Namilae	Member, Dr. Marwan S. Al-Haik
Member, Dr. Daewon Kim	
Graduate Program Coordinator, Dr. Marwan S. Al-Haik	Date
Dean of the College of Engineering, Dr. Maj Mirmirani	Date
Associate Provost of Academic Support, Dr. Christopher Grant	Date

Marwan Al-Haik
Digitally signed by Marwan Al-Haik
DN: cn=Marwan Al-Haik, o=Embry-Riddle Aeronautical University, ou=Aerospace Engineering, email=alhaikm@erau.edu, c=US
Date: 2020.12.03 18:08:04 -05'00'

Daewon Kim
Digitally signed by Daewon Kim
Date: 2020.12.03 15:50:00 -05'00'

Marwan Al-Haik
Digitally signed by Marwan Al-Haik
DN: cn=Marwan Al-Haik, o=Embry-Riddle Aeronautical University, ou=Aerospace Engineering, email=alhaikm@erau.edu, c=US
Date: 2020.12.03 17:14:41 -05'00'

Maj Mirmirani
Digitally signed by Maj Mirmirani
Date: 2020.12.04 09:31:41 -05'00'

Christopher Grant
Digitally signed by Christopher Grant
Date: 2020.12.04 09:41:12 -05'00'

ACKNOWLEDGEMENTS

Foremost, I would like to express my most tremendous appreciation to my advisor, Dr. Sirish Namilae, who consistently provides me with his knowledge, patience, assistance, and encouragement in my master's journey. His guidance is priceless for motivating me to achieve my thesis in the right direction. I would also like to thank Dr. Marwan S. Al-Haik for his advice on this research's broadness and Dr. Daewon Kim for his inputs on valuable aspects.

I would especially appreciate my parents for raising me and support me in chasing my dreams. My mother forever put me on her priority with tireless care from my childhood, and my father always stood by my side, giving endless support. They have sacrificed their life for me providing their infinite and unconditional love. I appreciate their education, and I appreciate my fate for being their son. They are my harbor and my shield wherever I go in the future.

I would also thank all my families for this precious opportunity of studying abroad. Being in America would be an unreachable dream without your generosity from the beginning of my journey. A special thank goes to my sister, Jiayi, for all the mental support and moments she stood by my side.

My gratitude also goes to my research group mates, Sandeep Chava, Samarth Motagi, and Audrey Gbaguidi, for their help throughout my work and for the fun we had together.

Last of all, I would sincerely thank all my best friends, Shurui, Tong, Yi, for their encouragement and concern, for all moments we shared together over the ocean and for our friendship over the past years.

ABSTRACT

The spreading of metallic powder on the printing platform is vital in most additive manufacturing methods, including direct laser sintering. Several processing parameters such as particle size, inter-particle friction, blade speed, and blade gap size affect the spreading process and, therefore, the final product quality. The objective of this study is to parametrically analyze the particle flow behavior and the effect of the aforementioned parameters on the spreading process using the discrete element method (DEM). To effectively address the vast parameter space within computational constraints, novel parameter sweep algorithms based on low discrepancy sequence (LDS) are utilized in conjunction with parallel computing. Based on the parametric analysis, optimal material properties and machine setup are proposed for a higher quality spreading. Modeling suggests that lower friction, smaller particle size, lower blade speed, and a gap of two times the particle diameter result in a higher quality spreading process. In addition, a two-parameter Weibull distribution is adopted to investigate the influence of particle size distribution. The result suggests that smaller particles with a narrower distribution produce a higher-quality flow, with a proper selection of gap. Finally, parallel computing, in conjunction with the LDS parameter sweep algorithm, effectively shrinks the parameter space and improves the overall computational efficiency.

TABLE OF CONTENTS

LIST OF FIGURES

Figure Page

Figure Page

LIST OF TABLES

SYMBOLS

D	=	Particle diameter
e	=	Coefficient of restitution
E_0	=	Realistic Young's Modulus
E^*	=	Equivalent Young's Modulus
G_0	=	Shear Modulus
G^*	=	Equivalent Shear Modulus
H	=	Particle position height
K_n	=	Elastic coefficient in normal direction
K_t	=	Elastic coefficient in tangential direction
m_i	=	Mass of particle_i
m^*	=	Equivalent mass of particle_i
R_i	=	Radius of particle_i
R^*	=	Equivalent radius of particle_i
S_n	=	Normal stiffness
S_t	=	Tangential stiffness
v	=	Blade speed
$v_{n_{ij}}$	=	Relative particle velocity in normal direction
$v_{t_{ij}}$	=	Relative particle velocity in tangential direction
v_x	=	Particle velocity in x-direction
w	=	Blade width
α	=	Adjustable parameter in Weibull distribution

β	=	Adjustable parameter in Weibull distribution
γ	=	Adjustable parameter in Weibull distribution
γ_n	=	Damping coefficient in normal direction
γ_t	=	Damping coefficient in tangential direction
ν_0	=	Poisson's Ratio
μ	=	Sliding Coefficient
ρ	=	Particle density
δn_{ij}	=	Particle overlapping in normal direction
δt_{ij}	=	Particle overlapping in tangential direction

ABBREVIATIONS

ABM	Agent-based Modeling
DEM	Discrete Element Method
DLS	Direct Laser Sintering
EBM	Electron Beam Melting
LDS	Low Discrepancy Sweep
MFR	Mass Flow Rate
SLM	Selective Laser Melting
SLS	Selective Laser Sintering
PBF	Particle Bed Fusion

1. Introduction

Additive manufacturing has drawn a great deal of attention in recent times. Numerous advances in the past decade have led to additive manufacturing applications in multiple fields such as engineering (Tepylo et al., 2019), robotics (Manfredi et al., 2013), and biology (Moreno et al., 2019). One of the most significant advantages of additive manufacturing lies in the ability to create optimized structures (Strano et al., 2013). For example, in Figure 1.1, the internal structure of the additive manufactured product has been optimized to exhibit higher tensile strength (Yadroitsev et al., 2007). Additive manufacturing answers the need for higher flexibility in designing complex structures. It can provide not only multiple solutions but also an optimized solution for designers.

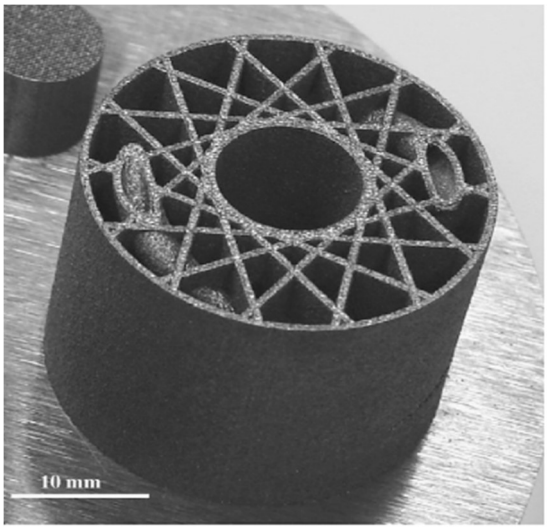

Figure 1.1 Structure optimization with additive manufacturing (Yadroitsev et al., 2007).

Depending upon the raw material type, additive manufacturing can be classified as liquid, discrete particle, and solid sheet based approaches (Vayre et al., 2012). One of the most typical examples of discrete particle material is metallic particles. To satisfy higher strength needs and reduce difficulties with oxidation, metallic particles, such as stainless

steel particles and titanium particles, are commonly used (Froes & Dutta, 2014; Luecke & Slotwinski, 2014). The general idea in metallic additive manufacturing is similar to manufacturing with other raw material types, which is gradually laying the material up and binding these layers together by sintering or melting (Harun et al., 2018). The performance of the final product depends on particle properties and the laying up process among other factors. Compared with conventional metallic manufacturing, metallic additive manufacturing provides more accurate control and less material waste during manufacturing (Watson & Taminger, 2018). Considering the specific design need or factors such as cost, there are many metallic raw material choices and the additive manufacturing techniques available for any given application (Zhang et al., 2016). Due to these advantages, metallic additive manufacturing is getting more attention from designers and is quickly becoming the next-generation technology in many industries.

Whether metallic powder or polymeric material is used, most additive manufacturing involves two continuous procedures: particle spreading and particle bonding. Several modeling techniques such as computational fluid dynamics (CFD) modeling (Tan et al., 2019), Finite Element Method (FEM) modeling (Schoinochoritiset al., 2016) have been used to describe the particle flow behavior in the additive manufacturing process. Among those, the Discrete Element Method (DEM) is particularly effective in modeling granular materials allowing a detailed investigation of 'micro' behavior (Shmulevich, 2010). The algorithm of DEM is similar to molecular dynamics, and it was first proposed to study the force interaction between nine circular disks under varying pressure (Cundall & Strack, 1980). The DEM has been utilized in many applications such as simulations for rock

fragmentation (Camones et al., 2013), pharmaceutical mixing or segregation (Yamane, 2004), and granular flow behavior involving heat transfer (Kruggel-Emden et al., 2006).

Many parameters affect the particle spreading quality in metallic additive manufacturing processes. These parameters can come from either material property or the machine setup. Optimizing some of these parameters can produce higher-quality particle spreading, resulting in higher printing quality, which is the primary motivation for the modeling and parametric analysis work in this thesis. A scientifically rational parametric analysis requires a large number of values to support the conclusion, which leads to a too high computational cost. For example, varying ten values for five parameters would result in a parameter space of 10^5 variations. Therefore, an algorithmic solution for reducing the required number of simulations while covering the parameter space effectively is also considered in this work. The second motivation for this work is to explore the application of novel parameter sweep algorithms to the parametric analysis in this problem.

The primary objectives of this thesis are the following:

(a) Develop and model for the particle spreading process and the various parameters that affect it using the discrete element method.

(b) Systematically vary parameters and analyze the DEM simulations to understand the influence of each parameter.

(c) Utilize a low discrepancy sequence (LDS) algorithm for parameter sweep to significantly improve the efficiency of the parameter sweep. This is the first application of LDS to a DEM model.

(d) Summarize and propose future work that can extend this research

2. Scientific Background and Literature Review

In this chapter, general principles of metallic additive manufacturing is introduced. The direct laser sintering is selected to describe the manufacturing procedure more specifically. The modeling for simulations is firstly presented and justified for its effectiveness from some previous studies. Additionally, the statistical tool adopted here is evaluated by some relevant researches.

2.1. Additive Manufacturing Processes

Additive manufacturing refers to a group of technologies that enable the building up of 3D objects layer by layer. Due to the recent advances in 3D printing technologies and CAD software, additive manufacturing is more frequently used to fabricate complex high-end products such as aircraft engine nozzles, artificial bones and joints (Seidel et al., 2019; Grayson et al., 2010). The term “additive” in additive manufacturing comes from the commonly seen laying-up procedure during the fabrication where each layer adds up to a three-dimensional product. Such a manufacturing process can be contrasted to conventional ‘subtractive’ manufacturing processes such as machining, where the final design is achieved by removing material.

Traditional subtractive manufacturing usually requires a large piece of raw material as the basis. The general idea of subtractive manufacturing can be revealed by the name, which is to create some structures by removing the material in a specific area as determined by the computer CAD program. As readily seen in the procedure, a fundamental subtractive manufacturing shortage lies in the input material. On the one hand, depending on the final design of the product, the raw material should be large enough to accommodate the final design. On the other hand, it is uncommon that the

removed material can be recycled for another design, which leads to a colossal waste in the manufacturing process (Hermez et al. 2019). Another shortage of subtractive manufacturing lies in the limitation of final product complexity. To generate a product with more complex structures, most situations combine both the subtractive manufacturing and additive manufacturing processes, which provide intricate designs but lead to a higher cost (Campbell et al., 2012).

These shortcomings have been overcome through recent developments in additive manufacturing. Firstly, the raw material used in additive manufacturing comes in the form of very fine powders or as a thin sheet. Such input material allows the manufacturing process to be eco-friendly by using the material as needed. The principle of the bonding procedure in additive manufacturing is to bond layers of input material according to the design. In this way, unbonded materials are commonly available to be recycled for another design, which greatly minimizes the waste in the manufacturing process. Besides, adding the material layer by layer allows for higher design flexibility at a reasonable cost (Hermez et al. 2019).

Years of research in additive manufacturing have led to the development of various manufacturing techniques to meet different requirements. When the application does not require high strength or stiffness, polymeric materials such as polymeric composites are widely chosen as filament material. One of the advantages of polymers over metallic materials is that the final product's property can be relatively easily modified by changing the property of the input material (Yuan et al., 2019). Specific additive manufacturing methods are useful for a given material type. For example, selective laser sintering (SLS) technology is mostly used for higher strength engineering thermoplastics such as nylon

(Beecroft, 2016). Fused deposition modeling (FDM) is more widely used for consumer products using thermoplastics such as PLA and ABS (Ahn et al., 2002; Mohamad et al., 2016; Drummer et al., 2012).

2.2. Direct Laser Sintering

When it comes to metallic additive manufacturing, there are various techniques to choose from for the particle bonding procedure. Some standard metallic additive manufacturing techniques include direct laser sintering (DLS), electron beam melting (EBM), selective laser melting (SLM), and binder jetting (Harun et al., 2018).

Most of the difference lies in the particle bonding process. The principal of metallic particle bonding is either to melt the particles by providing highly concentrated energy or bond particles together by inserting binder material. The aforementioned three commonly used techniques are all based on particle melting (Harun et al., 2018). All three techniques require highly-concentrated energy input; however, DLS requires lesser energy than EBM and SLM since it does not require all metallic particles to completely melt to bond with neighboring particles. Instead, only a portion of the particle will melt, and there remains a core formed by the unmelted particle portion. This detailed process was described in Zhu et al. (2003) and other DLS mechanism studies. (Simchi, 2006; Simchi et al., 2003).

In contrast, the mechanism of particle bonding in EBM and SLM requires particles to melt completely. In this case, only limited filament types are available because the material melting point and energy input have to be taken into account (Patterson et al., 2017). The modeling work on this thesis corresponds to the particle spreading process in approaches based on the particle bed fusion (PBF) like direct laser sintering.

Depending on the quality requirement of the final printed product, the detailed process of DLS varies for different printers. For example, it has been shown that adding the infiltration process produces parts that have lower residual stress and a higher printing quality (Vayre et al., 2012). The simplified process of DLS is illustrated in Figure 2.1.

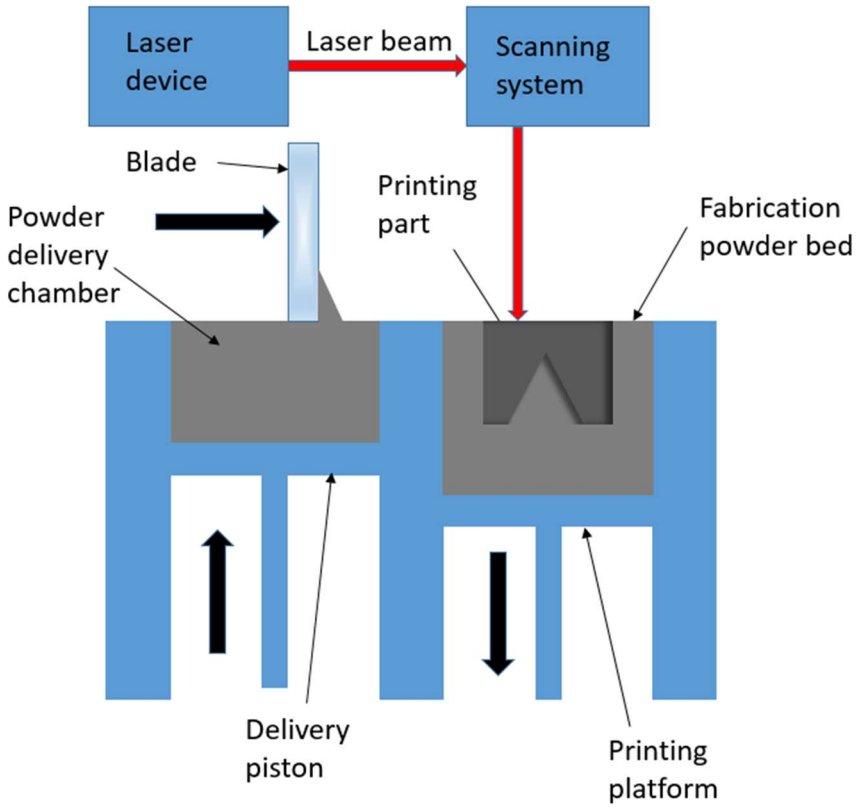

Figure 2.1 Schematic of direct laser sintering.

The set-up commonly consists of two different chambers, a powder delivery chamber and a printing chamber (Nandy et al., 2019). Metallic powder is input in the delivery chamber and is continuously provided by the delivery piston during the printing process. At the same time, a blade moves laterally, collecting some particles to the printing platform. By this process, a new layer of particles is spread on the printing platform. For particle bonding, a laser device generates a highly-concentrated laser beam. By working

along with the scanning system, the laser beam can sinter powders in specific areas according to the CAD design. After one layer is printed, the printing platform moves downwards, and a new printing cycle starts until all layers are printed.

Due to the great potential of DLS for industrial applications, many studies deal with the optimization of the DLS process. It has been proved that the quality of the laser sintering process can be optimized by controlling the laser scanning rate or input energy density (Han et al., 2019). But some aspects that need further attention are the influence of particle size distribution, particle layer thickness, etc., which can be categorized as the properties of the powder bed (Averardi et al., 2020).

Experimental studies have indicated that the quality of the particle spreading directly influences the final printing quality. Ziegelmeier et al. (2015) studied the effect of particle size and particle flow behavior on the printed part quality. They picked out particles from specific size ranges to create different size distributions. The result suggested that a higher flow efficiency and packing efficiency allows for a tighter printed structure. The study indicated that optimum particle size distribution with higher flowability can create parts with lower surface roughness and less void volume as well as lower porosity. In addition, Lu & Reynolds (2008) studied the effect of particle printing layer thickness on printing integrity and accuracy in TiNiHf alloy additive manufacturing process. In their work, breaking strength was used for describing the printed part integrity. The result suggested that $35\mu m$ layer thickness can achieve the best printing performance obtaining the highest breaking strength and the most accurate printing. The optimal layer thickness exists due to the balance of time for the binding process in lateral and vertical directions.

2.3. Particle Dynamics Modeling using Discrete Element Method

Particle dynamics is a sub-discipline of mechanics and dynamics that describes and analyzes the behavior of individual particles in a complex system. The particle is not only limited to solid granular particles but also includes fluid particles with an example of modeling a fluidized bed (Liu et al., 2017). In general, the idea of discretization is used in DEM, which is similar to the principle of the Finite Element Method (FEM). In both cases, modeling is considered effective in studying the macroscopic behavior of the system. DEM is effective in modeling discrete materials such as particles, whereas FEM is effective for analyzing materials and structures as continuous media (Munjiza et al., 1995). In some cases, a hybrid combination of FEM and DEM can be applied to study the behavior of granular structures (Azevedo & Lemos, 2006). By discretizing a complex system, a natural advantage of DEM comes from a detailed description of the behavior of the dynamical network.

The key to a realistic simulation of particle dynamics lies in the interaction between individual constituents, which is the basis of DEM. The principal of DEM is to observe the microscopic cluster behavior by defining the interaction between the constituent elements in the cluster (Shmulevich, 2010). By defining the interaction between particles, the state variables of a particle, such as the velocity, are changed based on a contact model. Such a change of the velocity can be further differentiated to obtain acceleration and the position based on Newton's Second Law. A general flowchart of DEM can be illustrated in Figure 2.2.

In DEM, particle status is determined by the interaction between two contacting particles. Such an idea of interaction and such application of Newton's Second Law is not

only seen in DEM. In molecular dynamics (Rapaport, 2004), the interaction between two particles is based on internal energy. Similar to DEM, the motion of molecules and atoms are updated by the integration of Newton's Second Law among the timestep. Additionally, in pedestrian dynamics (Helbing & Molnár, 1995), the interaction between two pedestrians is defined based on some social force model, which borrows many algorithmic features from DEM and molecular dynamics (Wąs et al., 2006). Here again, the position of each pedestrian is achieved by the integration of Newton's Second Law.

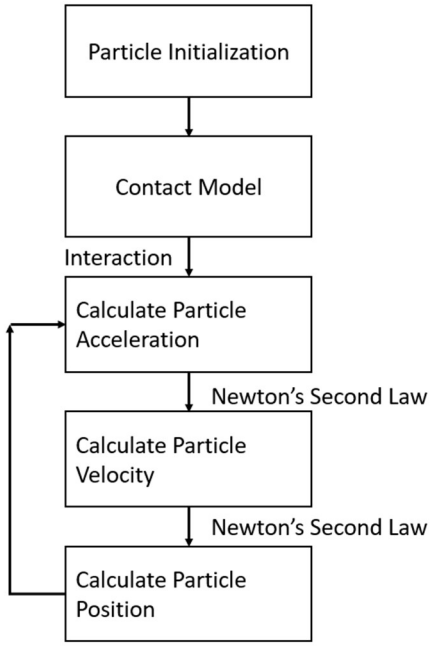

Figure 2.2 General procedure of DEM.

To describe the realistic behavior of particles in DEM, various contact models have been developed in the past few decades. Originally, when DEM was first proposed, the contact model between two individual disks is defined based only on the velocity of the boundary (Cundall et al., 1980). Later, contact models incorporate both force and velocity in the inter-particle interactions (Peng, 2014).

It is essential to choose a contact model based on the specific objective due to the sensitivity of contact models to simulation parameters. For example, the selection of soft deformable particles or hard rigid particles can reveal the sensitivity of the result to the contact models (Peng et al., 2014). Besides, there is a balance between the accuracy of the contact model and the computational cost. For example, a linear contact model with rigid interaction is computationally efficient. However, adding the cohesion or the energy dissipation can lead to a higher accuracy with significantly more computational cost (Di Renzo & Di Maio, 2004). This characteristic of the contact model has been a problem when performing DEM, as the balance between the accuracy and computational effort has to be considered to choose a proper contact model.

Another issue is the computational cost of the simulation setup. For example, the value of Young's Modulus when simulating the metallic particles can significantly influence the computational cost. Some previous works have also observed a significant increase in the computational time when using the real particle mass in DEM simulations (Lee et al., 2018; Lommen et al., 2014). Some previous works also manually set up the kinematic energy to zero so that the computational time can be reduced, obtaining an insensitive result even if the situation is unrealistic (Xiang et al., 2016). In such cases, the compromise between accuracy and computational cost should be considered when designing DEM simulations.

2.4. Particle Spreading Simulations

The powder bed in DLS is directly formed by laying up of the metallic particles. The particle flow behavior which can be correlated directly with the powder bed properties has drawn significant attention from researchers. Metallic particle diameters can be

extremely small, ranging from $5\mu m$-100 μm, and contain irregular shapes, which increases the difficulty in particle flow behavior studies. DEM is widely used, especially in particle flow behavior studies in metallic additive manufacturing.

Haeri (2017) optimized the blade shape in particle spreading using DEM. A super-elliptic shape was chosen as the blade profile. Solid volume fraction (φ_s) and surface roughness (ε) are modeled as the index of printing quality. Multi-sphere Approximation (MSA) was developed to generate particles for performing DEM. The results indicate that shorter and wider profiles lead to higher quality. Also, increasing the width of concave and convex blades results in opposite variations ofφ_s. Finally, the optimized blade and roller were compared to spreaders at the same spreader velocity. The sensitivity of the optimized blade to the spreading velocity was less than the sensitivity of a roller. This indicates that the optimized blade leads to a higher spreading speed and a higher manufacturing rate.

Nan et al. (2018) investigated the particle jamming behavior on the printing bed and studied the relation between empty patches in the printed bed and the location of spreader using DEM. In their work, all parameters used in the simulation were obtained by a series of experiments, including particle indentation for modulus and impact experiment for interfacial surface energy. The result indicated that for particles in front of the blade, particle motion is dominated by the shear band whose width depends on the blade speed. For particles under the blade, a negative velocity was observed, which was described as a dragging effect from the blade. The total number of pores decreased sharply with an increase in gap height. Additionally, the jamming frequency and jamming survival duration were negatively correlated with the formation of pores.

Parteli and Pöschel (2016) conducted DEM simulations to investigate the interaction between the printed part and the spreader in the particle spreading. A multi-sphere method was used to approximate the realistic shape of particles. Observing the force transmission of particle flow, they found a phenomenon that certain particles may carry more stress, whereas others carry much less, which was described as a force chain and was due to a varying distribution of cohesive forces between particles and particle shapes. Additionally, the result suggested that a higher spreader speed leads to higher surface roughness. Smaller particle sizes can lead to a higher surface roughness, which was explained by the tendency of smaller particles forming randomly shaped groups.

Haeri et al. (2017) studied the relationship between the fabrication process and printing performance using DEM. A multi-sphere technique was used to create the overlap of certain spherical particles to simulate the real particle shape in their work. The results indicate that the roller spreader performed better than the blade due to a larger contacting area and less particle dragging effect. When only considering the particle aspect ratioA_r, φ_s will reach a peak around $A_r = 1.5$, whereas ε will increase continuously. Additionally, the higher the spreader speed, the worse the printing performance.

Nan and Ghadiri (2019) utilized DEM to study the influence of the gap between the blade tip and powder bed and blade speed. The result indicated the same increasing trend of particle speed in their previous study (Nan et al. 2018), but a further explanation of the shear band was given. When increasing blade speed and decreasing the gap, the center of the shear band moves downward, and the width increases, affecting more particles. However, the shear band center position is less affected by gap height when the blade is

moving at a higher speed. Mass of particle flow increases with a higher blade speed, but a peak performance exists depending on the blade speed. Besides, a critical gap height with a value around particle diameter exists, cutting off particle flow, and the gap height should always be larger than two times of particle diameter to efficiently spread particles.

Han et al. (2019) studied layer thickness in particle spreading with DEM. Voids on the printed section can be reduced by increasing layer thickness due to a better particle flowability. After increasing the layer thickness to a certain extent, resilience can be observed due to the reduced compression between the spreader and the printing bed. For multi-layer printing, the printing quality was improved significantly because of the spatial interaction between particles in different layers. However, if layer thickness goes too high, a short feed phenomenon resulted from insufficient particle supply occurs at the end of printing. Therefore, an optimum layer thickness exists to balance the printing rate and particle short feed.

Lee et al. (2018) studied the particle packing density in the spreading process using the DEM model. A mass scaling method considering reducing the incremental time step was utilized to reduce actual particle mass also to improve calculation efficiency and accuracy. As for outputs, apparent packing density and voxel packing density were defined for describing packing structure. Particle size distribution tests with equal-sized, positively skewed distribution and Gaussian distribution was analyzed. The result suggested a higher fraction of smaller particles leads to higher packing density.

Xiang et al. (2016) correlated the packing density and the coordination number with the particle size distribution, the layer thickness, and the compression from the spreader. Simulations involved three different particle size distributions with the same mean radius

but various layer thickness for each distribution. The result suggested outputs do not vary much under different size distributions. However, with a larger layer thickness, both the packing density and the coordination number increase with a similar trend, and mono-size distribution produces the highest packing density and highest coordination number. Within the compression procedure, all the parameters tend to stabilize, which suggests the compression can improve the packing behavior and limit the randomness of packing.

Deng and Davé (2013) used a multi-sphere method in DEM to study the relationship between aspect ratio, particle size, surface energy, and porosity. For non-cohesive particles, porosity almost remains constant independent of particle size. When increasing surface energy, porosity increases, but the influence becomes weaker for larger particles due to the larger gravity. For non-cohesive particles, porosity increases due to larger particle size and higher surface energy. Also, for spherical non-cohesive particles, the coordination number decreases for higher surface energy. For spherical cohesive particles, the coordination number increases, indicating a lower porosity. Also, the porosity increases for smaller particle sizes and higher aspect ratios.

Bai et al. (2015) studied the methodology to improve sintered part density and powder bed density by varying bimodal particle size distribution. The result suggested the existence of large particles can improve both printing bed density and printed part density, which guides to optimize particle size distribution width without changing the mean size. However, this improvement was restricted by extra-large particle forming a rigid skeleton. Besides, optimized bimodal size distribution can contribute to reducing the volume shrinkage of the printed part after sintering.

Karapatis et al. (1999) studied the relation of particle composition and layer density by controlling the fraction of different sized particles. In the research, they proposed a formula for estimating the preferred composition for higher density. These numerical values matched well not only with their experimental study but also for some previous studies. Additionally, the total void volume fraction in the powder bed caused by the wall effect can be evaluated concerning the particle radius and the layer thickness. By increasing the smaller particle volume within a certain fraction range, the powder bed density can gradually increase.

Chen et al. (2017) simulated flow behavior in particle spreading using DEM. In their work, the dynamic repose angle (DRA) describing the dynamic profile of the particle pile was defined to indicate flow fluidity. When increasing particle surface energy density, the particle flow turns discontinuous and unstable, leading to some large pores on the printed part. A higher friction coefficient can reduce fluidity. When not considering cohesion, decreasing particle size can attribute to better fluidity, continuity, and stability. However, if cohesion exists, the decrease of particle size has a lower boundary. Additionally, the spreading speed and the gap size do not have a significant influence on fluidity, but increased blade speed and decreased gap size can significantly deteriorate flow continuity and stability.

Based on these previous studies, the quality of spreading can be considered to be a vital factor in overall printing quality. But the limitation of these previous works is, in each work, only one material with fixed parameters was simulated. However, in reality, there are numerous choices for input material properties and process variables. Therefore, in this parametric analysis, instead of a single value, a small range of numerical value is

given to each parameter to analyze the varying trends corresponding to all parameters. This can be considered as a novel contribution to this work.

Additionally, when it comes to the effect of the particle size, not only uniform particles but also mixed particles may play a role in the particle spreading quality. In reality, due to the manufacturing process, it is extremely hard to find some uniform-sized particles when it comes to the fine powder. The particle size distribution can have both positive and negative effects, as suggested in the following previous studies.

Spierings et al. (2011) investigated the influence of the metallic particle size distribution in additive manufacturing. From a previous study of their own, three different types of particle distribution were created, including a different fraction of large particles. In their work, surface roughness was introduced to evaluate the performance of the fabrication. The result suggested that a higher fraction of large particles tend to increase the surface roughness of the final product, which is considered as a negative effect. Additionally, the mechanical properties such as the tensile strength were also investigated, which indicates the existence of course particles can benefit the mechanical properties to a varying extent depending on the layer thickness.

Siniko et al. (2019) proved the effect of the particle size distribution of Maraging 300 powder in Laser Powder Bed Fusion. With a sequence of preliminary analyses, two of three types of size distribution with a slight difference in the mean size were finally studied. As a result, an observation of a relatively higher porosity is presented, which is explained due to a narrower distribution of particles. Besides, the surface roughness of the top and side of the printed part was studied as well. The result indicated that a particle size distribution with a slightly smaller mean size tends to obtain a lower top surface

roughness. A remelting process with a specified layer thickness was proposed to be effective in lowering the surface roughness and improving the surface quality.

Based on these previous works involved with the particle size distribution, the most common way of obtaining the distribution by experiments is to observe the distribution of particles in a 2D plane. Then the overall size distribution in 3D space can be approximated. Some inter-layer distributions can be lost when converting the layer distribution to spatial distribution, which leads to an error of analysis. Despite the limitation, the method is still popular among experimental studies due to the ease of performing particle size observation in a plain (Fang et al., 1993; Nan et al., 2018).

Another approach for obtaining the particle size distribution is to describe the particle variation by some mathematical distribution models. For example, Fang et al. (1993) investigated the particle size distribution analytically based on the experimental data. In their work, the Weibull function was used for data fitting. The frequency distribution fitting procedure was performed by an optimization algorithm based on the direct searching method and then unfolded into the realistic size distribution. The result suggested that the proposed Weibull distribution fit the raw particle size distribution well, which can be a potentially substituting method for the conventional way of finding the particle size distribution by the 2D distribution image.

Note that describing the particle size distribution by a mathematical distribution model is empirical and does not have a strong theoretical basis (Fang et al., 1993). However, it can be an effective way to describe particle distribution when it comes to a large number of samples. In such cases, the experimental procedure can be accurate but more time and labor-consuming compared with the analytical particle distribution study.

2.5. Parameter Sweep Algorithms

Parameter sweep is a well-developed methodology that has been commonly used in statistical analysis. A significant application of parameter sweep algorithms is to shrink the original parameter space while allowing parameters to cover the entire parameter space efficiently. Three commonly seen are lattice-based sweep, random sweep, and low discrepancy sweep. The parameter coverage for a 2D parameter space is described in Figure 2.3.

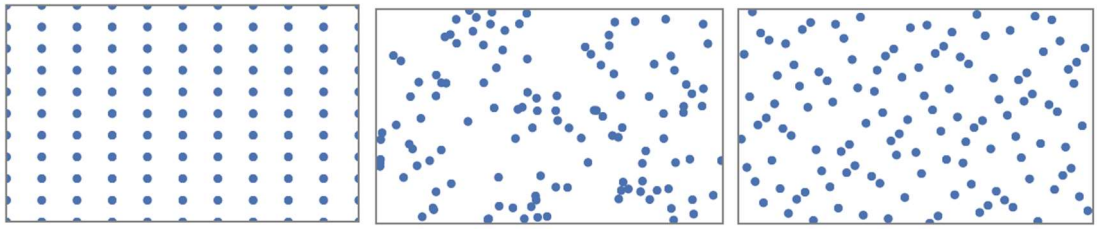

(a) (b) (c)

Figure 2.3 Parameter Sweep Coverage of (a) Lattice Space (b) Random Space (c) LDS Space (Chunduri et al., 2018).

Parameter coverage in a lattice-based algorithm is generally considered not efficient. As shown in Figure 2.3 (a), the blank part is uncovered parameter space, and each grid represents a set of parameters. Apparently, in any parameter sweep, there will always be some blank part. Therefore, efficient coverage can be described when the distances between any of the two neighboring grids are relatively the same (Chunduri et al., 2018). Additionally, lattice-based sweep doesn't provide an automatic convergence check. To check the convergence of the parameter space, a comparison between the current lattice and its sub-lattice has to be conducted. Due to the randomness of the sub-lattice space, a manual convergence check is inefficient.

Compared with a lattice-based sweep, a random sweep usually allows an automatic convergence check, which can save some computational cost. However, as shown in Figure 2.3 (b), the coverage of the new parameter space is inefficient, which has limited its utilization in statistical analysis.

Compared with the other two, Low Discrepancy Sweep (LDS) has shown great potential in reducing parameter space. The discrepancy is a term used for describing the cumulative deviation between current parameter distribution and ideally uniform parameter distribution. LDS has been commonly used due to the more efficient parameter coverage and the ability to automatically check convergence. This increases the computational efficiency of the algorithm. LDS has been used for many applications, such as the boost of the Monte Carlo method (Tuffin, 1996) and a stochastic optimization algorithm (Yang et al., 2015).

Chunduri et al. (2018) applied LDS in studying pedestrian infection behavior. A conventional lattice-based algorithm was compared with the LDS algorithm. The convergence in lattice parameter space was checked by manually comparing sub-lattice parameter space, whereas, in LDS, the convergence of pedestrian infection was checked by automatically comparing statistical parameters. Skewness and kurtosis were used for checking convergence. The result suggested that LDS can cover parameter space more efficiently and can significantly reduce the number of simulations to cover the parameter space.

Braaten and Weller (1979) firstly proposed a scrambled Halton sequence and utilized the new sequence for multi-dimensional integration. In their work, a strong correlation was observed when using the Halton sequence in a higher dimension, which was

described as due to the monotonically increasing numbers used for generating the sequence. The overall discrepancy of the scrambled sequence was much lower than the original Halton sequence. When applied in an integral calculation, the scrambled sequence shows a much faster convergence rate compared with traditional Monte Carlo calculation and produced much lower fluctuation in the integration error than the Halton sequence.

Rubio et al. (2015) applied the parameter sweep into an iterative optimization algorithm to simulate and find out the best energy distribution on an energetic island. In their work, two parameters were defined to describe the performance of the energy distribution, and the criteria for stopping algorithms were defined when two indicators go into an acceptable range. The original parameter space was randomly created, going through a sequence of optimizing algorithms. During each stage of the optimization, the parameter set value changes, leading to a reshape of parameter space and generating new simulation models. The result suggested the great effectiveness of parameter space in finding neighboring parameter values through the iterative steps of the optimization algorithm.

Kiss et al. (2010) utilized parameter sweep in recognizing carbohydrate for biological molecules. In their work, a user-friendly recognizing algorithm that contains parameter sweep was proposed. The algorithm combined parallel computing in molecular dynamics combined with a pre-defined parameter sweep aimed to process a large number of input files. Compared with the conventional method of recognizing large and complex bio-molecules requiring weeks up to months, parameter sweep, along with parallel

computing, allows run similar-sized jobs in 24-36 hours, which is a significant improvement.

Srinivasan (2002) compared the application of the Monte Carlo and the Quasi-Monte Carlo using various sequences, including low discrepancy sequences such as the Halton Sequence and the scrambled Halton sequence. It was stated that the convergence rate of the Quasi-Monte Carlo had been greatly improved with the utilization of the LDS due to the uniformity of QMC with LDS rather than the randomness of MC. The parallelization of QMC was studied to investigate the effect of various sequences. LDS was confirmed to have a good performance in low dimensions. However, when it comes to high dimensions, the performance of QMC can largely depend on the choice of the sequence. Certain sequences have poor performance in high dimensions with larger data space. However, such data distribution problems can be avoided by proper projections.

In this thesis, we combine aspects of low discrepancy parameter sweeps with the DEM model of particle spreading process to fundamentally understand the factors affecting the quality of the powder flow behavior in additive manufacturing.

3. Methodology

The flow behavior during the particle spreading can be difficult to fully investigate through experiments. The computational modeling using DEM is capable of detailed analysis of the complex interaction between particles in additive manufacturing. This parametric analysis focuses on the particle flow simulation in the context of additive manufacturing.

3.1. Contact Model

A variety of contact models have been proposed to mimic the realistic interactions between particles, ranging from small powders (Pantaleev et al., 2017) to larger granular objects such as rock (Jiang et al., 2015). A general classification of such models is based on the deformability of particles (Peng, 2014). A more detailed classification can be made based on the characteristic of the interaction of the particle property. For example, the microscopic cohesion effect concerning Van Der Waal force can be separately specified or combined to get into the most realistic particle interaction (Abbasfard et al., 2016; Gan et al., 2016)

In this work, the Hertz-Mindlin contact model is utilized to simulate the particle interaction. Hertz-Mindlin contact model is widely used for particle dynamics simulations for applications such as stress field description (Langston et al., 1994) and rotating drum simulation (Cheong et al., 2014). It is considered as a non-linear contact model that produces an accurate interaction between particles with an acceptable computational cost. Another commonly used contact model with the Hertz-Mindlin contact model is the Johnson-Kendal-Robert (JKR) cohesive model (Johnson et al., 1971). In such a model, the normal force between two particles is reduced by the Van Der

Waal force, which results in an energy transmission from kinematic energy to the particle elastic energy (Chen & Elliott, 2020). To consider the particle cohesion, the JKR contact model can be ported into the Hertz-Mindlin contact model. The behavior of smaller particles can be affected (Han et al. 2019; Nan et al., 2018).

In the Hertz-Mindlin contact model, the interactive force between any two contacting $particle_i$ and $particle_j$ can be calculated based on Equation 1 (Kloss et al., 2012).

$$F_{ij} = \left(K_n \delta n_{ij} - \gamma_n v_{n_{ij}}\right) + \left(K_t \delta t_{ij} - \gamma_t v_{t_{ij}}\right) \tag{1}$$

The total force between two particles is resolved into two directions, one normal to the line between two particle centers denoted by F_n and one tangential to the line denoted by F_t. In both two directions, the damping effect and elastic effect are considered. The elastic effect is described by elastic coefficients K_n and K_t with overlapping in two directions δn_{ij} andδt_{ij}. Similarly, the damping effect is described by damping coefficients γ_n and γ_t with relative velocity in two directions $v_{n_{ij}}$.and $v_{t_{ij}}$. Firstly, the material parameters used in the contact model can be calculated from realistic engineering parameters from Equation 2 to Equation 6.

$$E^* = \frac{E_0}{2(1-\nu_0)^2} \tag{2}$$

$$G^* = \frac{E_0}{4(2-\nu_0)(1+\nu_0)} \tag{3}$$

$$R^* = \frac{R_1 R_2}{R_1 + R_2} \tag{4}$$

$$m^* = \frac{m_1 m_2}{m_1 + m_2} \tag{5}$$

$$\beta = \frac{\ln(e)}{\sqrt{ln^2(e) + \pi^2}} \tag{6}$$

Whereas, R_1, R_2, m_1, m_2 denote the mass and radius of the two contacting particles. E_0 G_0 ν_0 denote the realistic Young's Modulus, Shear Modulus, and Poisson's Ratio. $E^* G^*$ $R^* m^*$denotes each equivalent parameter correspondingly. β is a coefficient related to the restitution coefficient e.

Further, the stiffness in the normal direction $S_n$and the stiffness in the tangential direction S_t can be obtained from Equation 7 and Equation 8,

$$S_n = 2E^* \sqrt{R^* \delta_n} \tag{7}$$

$$S_t = 8G^* \sqrt{R^* \delta_n} \tag{8}$$

where δ_n denotes the overlapping between two particles in a normal direction.

Lastly, the elastic coefficient and the damping coefficient can be calculated from Equation 9 to Equation 12.

$$k_n = \frac{4}{3} E^* \sqrt{R^* \delta_n} \tag{9}$$

$$\gamma_n = -2\sqrt{\frac{5}{6}} \beta \sqrt{S_n m^*} \geq 0 \tag{10}$$

$$k_t = 8G^* \sqrt{R^* \delta_n} \tag{11}$$

$$\gamma_t = -2\sqrt{\frac{5}{6}}\beta\sqrt{S_t m^*} \geq 0 \tag{12}$$

The contact model applied in this work can be demonstrated in Figure 3.1. The sliding friction is included in the tangential direction, which is one of the reasons for a relatively more accurate result compared with some linear contact models but can increase the computational cost as a side effect. The sliding coefficient is applied to truncate the tangential overlapping δt_{ij} by Equation 13.

$$F_t \leq \mu F_n \tag{13}$$

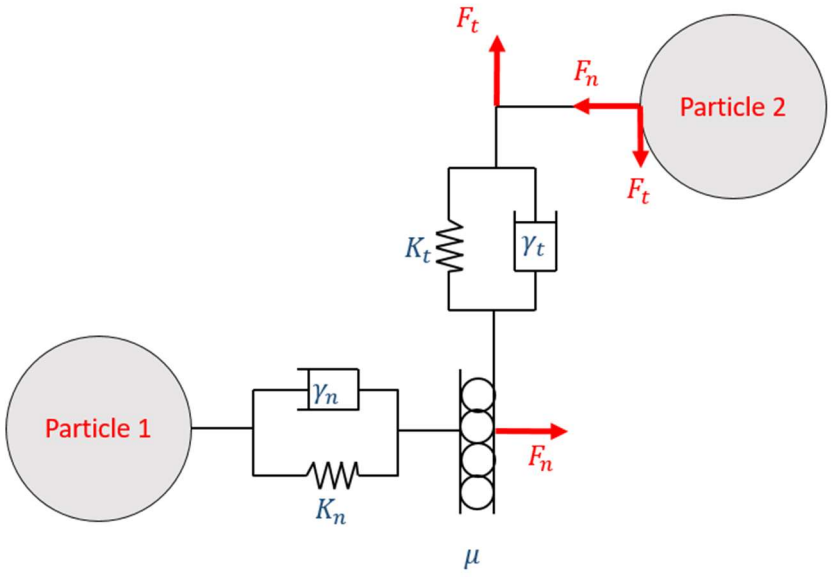

Figure 3.1 Hertz-Mindlin contact model.

3.2. DEM Simulation Setup

The DEM simulation software used in this work is called LIGGGHTS (LAMMPS Improved for General Granular and Granular Heat Transfer Simulations)

(Kloss et al., 2012). LIGGHTS adapts the LAMMPS molecular dynamics algorithms (Plimpton, 1995) to DEM modeling of granular solids. Also, similar to LAMMPS, LIGGGHTS is capable of coupling with visualization software such as Paraview and VTK, which can provide a straightforward macroscopic observation of the simulation. In this work, Paraview (Ahrens et al., 2005) is coupled with LIGGGHTS for the post-processing of the simulation data.

To describe details of DEM in this work, a flowchart is provided in Figure 3.2. At the beginning of the simulation, a certain number of particles with specific material parameters are inserted. The contact criterion is defined as: when the distance of two particle centers is less than the summation of two particle radius, there is contact between two particles. Both the position and the velocity of each particle are obtained to compare with the criterion. When the criterion is not reached, namely, when there is no contact between two particles, the motion of each particle is only based on the gravity and can be derived by Newton's Second Law. Thus, the updated position of two particles is provided with a timestep.

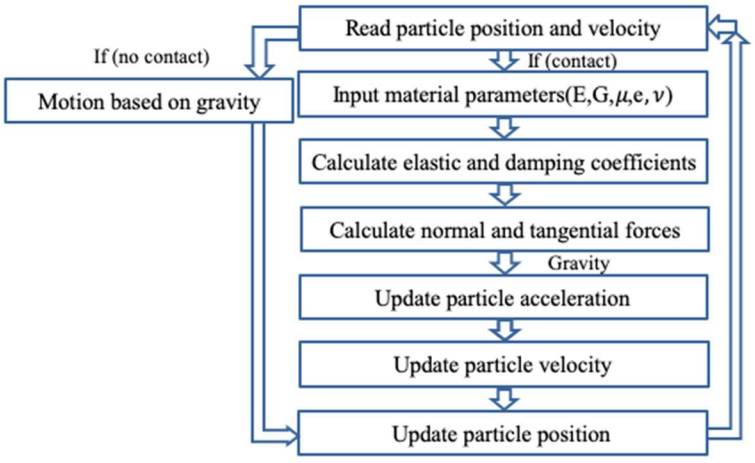

Figure 3.2 DEM flowchart.

When two particles are contacting, the DEM algorithm calculates the inter-particle forces based on the contact model. If there is contact between two particles, both the elastic force and the damping force are calculated based on particle property, as shown in Equations 2 - 12. The tangential contact force can be obtained from the normal contact force and a truncated friction coefficient. The effect of gravity is included, and the acceleration for each particle is evaluated using Newton's Second Law. This is followed by integration with a small timestep to determine updated velocities and the updated positions of two contacting particles.

To replicate the realistic particle spreading process, a rectangular geometry is inserted into the simulation box to mimic a blade spreader carrying some particles with varying speed from left to right. Figure 3.3 shows a partial magnification of the blade tip area. Some particles are accumulated in front of the blade. A gap allowing particles to go through is defined with the distance between the blade tip and the printing bed. The gap distance is one of the parameters studied in this parametric analysis. In this figure, a post-processing area is defined as well, which will be described in detail later.

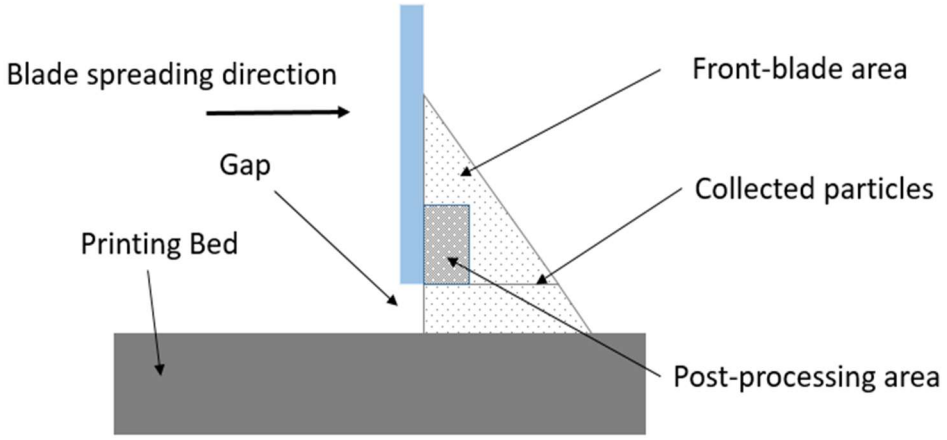

Figure 3.3 Blade tip area.

In this parametric analysis, in addition to the gap size, the inter-particle friction, the particle diameter, and the blade speed are also investigated. All parameters used in the DEM simulation are listed in Table 3.1.

Table 3.1

Simulation parameters.

Parameters	**Value**
Particle diameter, D (mm)	1, 1.5, 2, 2.5, 3
Particle density, ρ (kg/m^3)	7980
Young's modulus, E (GPa)	2.1
Effective Young's modulus, E (MPa)	21
Poison ratio, υ	0.3
Friction coefficient	0.1, 0.15, 0.2, 0.25, 0.3
Restitution coefficient	0.4, 0.45, 0.5, 0.55, 0.6
Gap size(mm)	1, 2, 3, 4, 5
Blade speed(m/s)	1.2, 1.3, 1.4, 1.5, 1.6

The average parameter values are obtained from a previous study (Nan & Ghadiri, 2019) using similar material. For example, for the four parameters studied in this work, a range is adopted rather than a single numerical value compared with previous studies. The modification aims to adjust the DEM simulation to this parametric analysis. In previous works (Nan & Ghadiri, 2019; Nan et al., 2018; Parteli & Pöschel, 2016), only fixed material with certain fixed parameters were used to investigate the flow behavior. However, in reality, the material property can vary with the filament type. Even for the same type of material from different manufacturers, the material property may vary as well. Thus, the variables in this work are given a small range based on the realistic value.

One thing to notice is that Young's Modulus used in this work is called the effective Young's Modulus which is two-order lower than the realistic modulus. This modification is to reduce the computational cost. A solution to properly balancing the simulation

accuracy and the computational cost is to reduce the order of the Young's Modulus within 10^2(Parteli et al., 2016). A more detailed discussion about such compensation is presented later in Section 5.1.

The focus of the thesis is to investigate the flow behavior in front of the blade or near the gap. A post-processing area in front of the blade, as shown in Figure 3.3, is identified as a representative post-processing area for this purpose. Nan & Ghadiri (2019) used a similar post-processing region for analyzing flow behavior.

The particle flow should be smooth and stable to produce a higher printing quality. This can be correlated to the distribution of the particle velocity of all collected particles in front of the blade. To be specific, a smooth variation of the velocity distribution along the direction of motion of the blade can indicate a smooth and stable particle flow. The output of the LIGGGHTS DEM simulation can be post-processed to obtain the resolved velocity of each particle along with detailed location coordinates. Defining the direction of blade motion as the x-direction and z-direction is perpendicular to the powder bed, the velocity of a particle in the x-direction is denoted byv_x. The v_x distribution among z-direction is described for the judgment of the particle flow smoothness.

Smooth distribution of v_x among different layers of particles is desired (Nan & Ghadiri, 2019). Note that the particle size and the height H of each layer to the blade tip are parametric variables in this study. Therefore, the layer location is defined by the average particle diameter D, which is defined as the relative height H/D. The distribution of particle speed v_x among the particles at a given height is chosen as the indicator of the particle flow smoothness. As shown in Figure 3.4, the dimension of the post-processing area is defined based on the particle diameter. The absolute dimension of the area can

change with varying particle size. However, by defining the relative height, the v_x parameter is standardized.

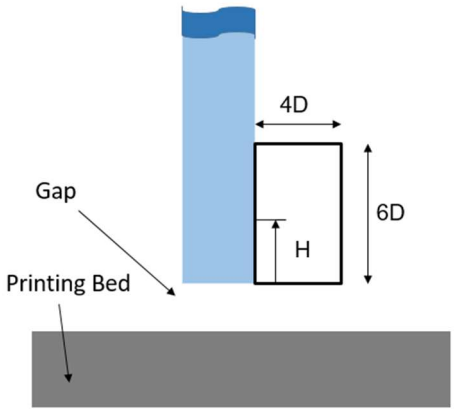

Figure 3.4 Post-processing area dimensions.

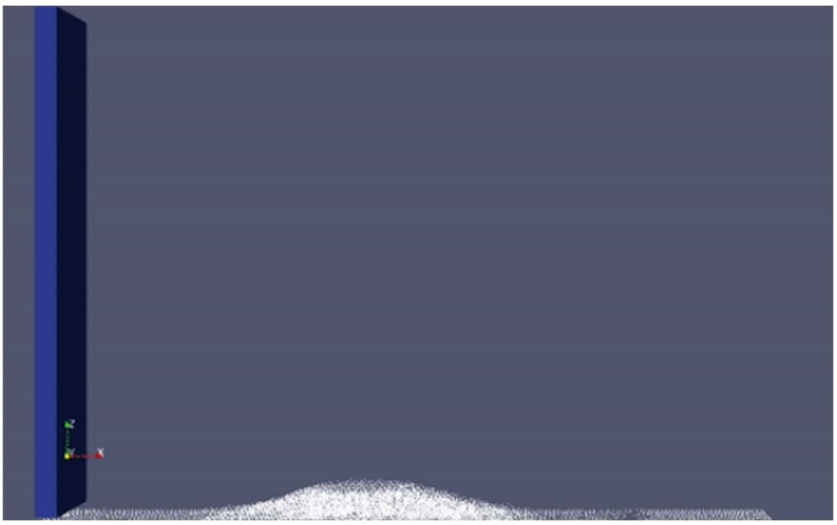

Figure 3.5 Initial setup of DEM simulation.

In all simulations, at the beginning of the simulation, particles are inserted into the insertion box which is located at the top of the simulation box. After particle insertion, all particles fall freely into the simulation box due to the effect of gravity. At the end of this step, particles form a pile with some random shapes depending on the particle number

and the particle size, as shown in an example simulation setup in Figure 3.5. This is not the same as the flat distribution of particles before the spreading procedure (Nandy et al., 2019). However, such two initial distributions share the same moment that particles interact with the blade forming a triangular pile in front of the blade. Therefore, in this work, only the interacting moment is considered to replicate the realistic spreading regardless of the original distribution of particles. This simplification aims to reduce the number of particles as many as possible, controlling the computational cost in an acceptable range. The flow behavior analysis in this work occurs in the middle of spreading, which guarantees full contact of the blade and particles, so that makes the flow behavior approach the realistic spreading.

A mathematical distribution model is used in this work to describe the particle size distribution. Numerous distribution models are used for describing the particle size variation. Applying the mathematical distribution models is considered to be an effective method for describing various-sized particles in the following studies.

Shirazi & Boersma (1984) and Buchan & Buchan (1989) used Gaussian distribution and lognormal distribution to describe the particle size distribution of the soil sample composed of clay, sand, and other textures. Similarly, a modified lognormal distribution was proposed by Wagner & Ding (1994) for evaluating the soil particle size distribution. Hartmann et al. (1988) applied log-hyperbolic distribution to investigate the particle size sorting and distribution. Pinnick et al. (2007; 1985) described the size distribution of dust particles that are generated by vehicles in traffic using bimodal distribution. In addition to microscopic particles, Kittleman (1964) used Rosin's distribution to fit the size distribution of rocks.

In this work, Weibull distribution is chosen due to its natural simplicity and versatility. The prototype of Weibull distribution was performed by Rossin & Rammler (1933) to describe the size distribution of the powdered coal. However, Weibull distribution was proposed officially later in Weibull (1951) to characterize the fragmentation of materials. It is believed that Weibull distribution and its integral form, namely, Rossin-Rammler distribution, are capable of quantitatively describing the size distribution of fragmentation among materials (Zobeck et al., 1999).

In previous studies, Weibull distribution has been widely used for characterizing the particle size distribution. For example, Wohletz et al. (1989) used Weibull distribution to describe the particle size distribution of volcanic ash. Boadu & Long (1994) used the Weibull distribution to describe the size distribution of broken rocks. A similar approach was used by Froehlich & Benson (1996), when studying the size distribution of dumped rocks. Additionally, Weibull distribution was applied to investigate the size distribution of the crushed ice particles (Tuhkuri, 1994).

The cumulative density function of particle size is an effective parameter for describing the distribution. Based on the relationship between the cumulative density function and the probability density function, most cumulative density functions are derived from the integral. An advantage of Weibull distribution is that the cumulative density function of the can be directly obtained from the self-defined parameters.

To be more specific, the number of particles that are larger than size x per unit volume can be evaluated by Equation 14 (Fang et al., 1993). In the equation, N denotes the total number of particles per unit volume, whereas α, β, γ are adjustable parameters controlling the shape of the Weibull distribution and can be determined directly by data

fitting, which should be easier than fitting the integral form of cumulative density function in other distribution models.

$$N_{>} = N * \exp[-\frac{(x-\alpha)^{\beta}}{\gamma}] \tag{14}$$

Another reason for the Weibull distribution being commonly used for describing the particle size distribution lies in the data fitting. Generally, it is feasible to apply other mathematical models such as lognormal distribution and normal phi distribution. However, such models require a logarithm conversion from the actual particle size, which could be a source of errors in describing the realistic size distribution.

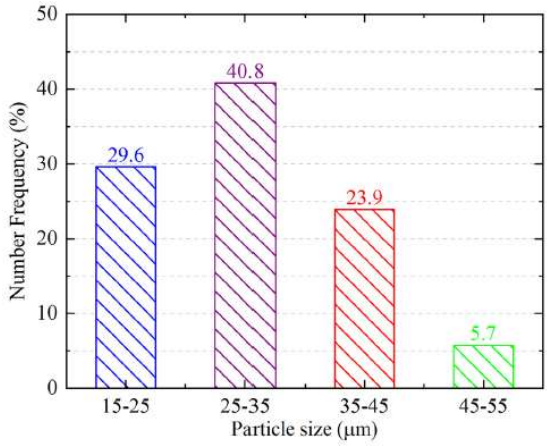

Figure 3.6 Realistic particle size distribution (Nan & Ghadiri, 2019).

In this work, the Weibull distribution parameters are obtained from a previous study (Nan & Ghadiri, 2019). In their work, the actual particle size distribution is obtained by observation of SEM, which gives the result shown in Figure 3.6. In such distribution, a data fitting procedure is performed to calculate the Weibull distribution parameters to mathematically describe the particle size distribution. The probability density function and the cumulative density function achieved by data fitting are shown in Figure 3.7.

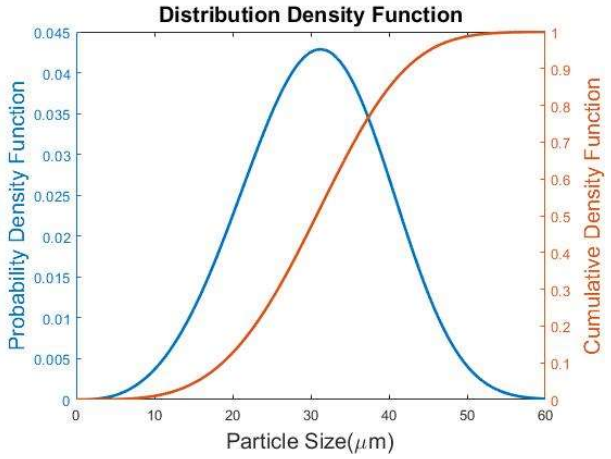

Figure 3.7 Numerical distribution function of the particle size.

Unfortunately, the particle size distribution function of LIGGGHTS is no longer available in the current version. Due to this limitation, a sequence of featured data points in the size distribution has to be provided. Considering the limitations of particle insertion and the probability density function, five featured particle diameters are chosen, and each corresponding fraction is obtained from the Weibull parameters. As done in the case of uniform particle size, the particle diameter is scaled up to make the simulation more computationally effective and comparable with other simulations in this work.

Note that the sample space given by the previous study can be described based on the particle size variation, which means the largest particle diameter is around two times the smallest particle diameter and is considered as a wide distribution. In this way, two kinds of particle distribution are used for given particle size. The first strategy is to use the same numerical relationship between the largest and the smallest particles to make this work comparable with the previous work (Nan et al., 2019), giving the same mean particle size. Then, the Weibull distribution is further modified into a narrower

distribution to indicate a higher quality metallic powder. Detailed distribution is defined in Section 4.6.

Additionally, to further investigate the relationship between the particle size distribution and the gap size, simulations are performed with a fixed gap size and with varying gap sizes for each case. The particle size and the gap size for simulations are given in Table 3.2 and Table 3.3. Detailed reasons for selecting these values will be discussed in Chapter 5.

Table 3.2

Particle diameters in strategy 1 with (a) uniform (b) varying gap size.

Fraction (%)	Particle Diameter(mm)				
	1mm	1.5mm	2mm	2.5mm	3mm
4.44	0.7	1.1	1.4	1.7	2
22.76	0.85	1.3	1.7	2.1	2.5
40.78	1	1.5	2	2.5	3
26.91	1.15	1.7	2.3	2.9	3.5
5.11	1.3	1.9	2.6	3.3	4
Gap(a)(mm)	5				
Gap(b)(mm)	2	3	4	5	

Table 3.3

Particle diameters in strategy 2 with (a) uniform (b) varying gap size.

Fraction (%)	Particle Diameter(mm)				
	1mm	1.5mm	2mm	2.5mm	3mm
4.44	0.8	1.3	1.8	2.3	2.8
22.76	0.9	1.4	1.9	2.4	2.9
40.78	1	1.5	2	2.5	3
26.91	1.1	1.6	2.1	2.6	3.1
5.11	1.2	1.7	2.2	2.7	3.2
Gap(a)(mm)	5mm				
Gap(b)(mm)	2	3	4	5	

The same procedure, as illustrated before, is utilized for post-processing. However, since the analysis is based on the uniform particle diameter, the selection of the average particle diameter is crucial. A general solution is adopted in this work, which is based on the cumulative density function of the particle size distribution. When translating the cumulative density function into the particle size distribution, for example, D_{90} denotes that 90% of particles' diameter is smaller thanD_{90}. Therefore, considering the cumulative density function as shown in Figure 3.7 (b), D_{85} is used for the post-processing, which happens to be the fourth featured diameter.

3.3. Parameter Sweep

To understand the effect of different parameters of the particle flow process, the parameter space is further expanded. Both lattice-based parameter sweep and LDS parameter sweep are conducted to compare the convergence rate and the computational efficiency of the parameter sweep algorithm. The lattice-based sweep is performed within the same numerical value range but giving varying intervals to create different lattice parameter space. The detailed parameter space is listed in Table 3.4.

Table 3.4

Lattice-based parameter space simulation parameters.

Parameter	**Range**	**Mesh 1**	**Mesh 2**	**Mesh 3**	**Mesh 4**	**Mesh 5**
Friction	0.1-0.3	5(0.045)	6(0.036)	7(0.03)	9(0.0225)	10(0.02)
Particle size(mm)	1-3	5(0.45)	6(0.36)	7(0.3)	9(0.225)	10(0.2)
Gap size(mm)	1-5	5(0.9)	6(0.72)	7(0.6)	9(0.45)	10(0.4)
Blade speed(m/s)	1-5	5(0.1125)	6(0.09)	7(0.07)	9(0.05625)	10(0.05)
Number of grid		625	1,296	2,401	6,561	10,000

Although simple to understand, lattice-based parameter sweep is computationally inefficient and requires significant computational effort. One of the common solutions to this problem is to run all simulations in parallel rather than in serial. To be more specific, tasks can be divided into several sections and are assigned to a certain number of processors depending on the job size and system utilization.

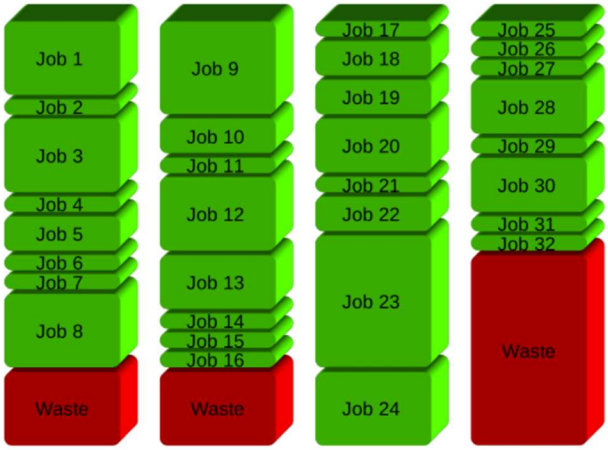

Figure 3.8 Conventional parallel computing task assignment (Tang, 2011).

Despite the improvement of the computing efficiency compared with serial computing, running jobs in parallel usually produces computational waste commonly due to the inactive processor, as shown in Figure 3.8. In other words, improper task assignments may lead to a different time for each processor to finish its section. But the total time needed for completing the task depends on the processor which is running the longest job. Therefore, the common situation is that one or two processors are still running the task, but the other processors may have finished their assigned tasks going into the inactive status and resulting in computational waste.

To optimize the simulation task assignment, a parallel computing tool called the GNU parallel is applied in this work. It is considered a powerful shell tool for processing a

large-sized job. The basic application of the GNU parallel lies in processing multiple tasks on multiple processors at the same time, which can be done by conventional parallel computing as well. However, a more flexible task assignment control of the GNU parallel is better than the other conventional parallel computing tools. For example, a computational space for running a large job can be limited as desired based on the system and the current computing resource distribution, which may provide an optimized utilization of the computing space to satisfy various conditions.

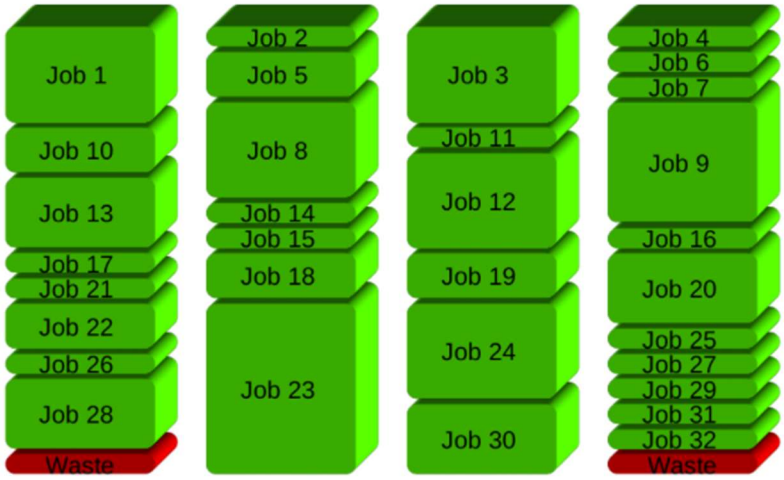

Figure 3.9 GNU parallel computing task assignment (Tang, 2011).

The greatest advantage of the GNU parallel is that it provides a smart solution to assigning tasks into multiple processors, as shown in Figure 3.9. Compared with traditional parallel computing tools assigning all tasks at one step, the GNU parallel will gradually assign tasks to processors one by one. With that being said, another task assignment is triggered after one job is done. The most direct result of this smart assignment is that the task distribution on each processor is changed, which reduces the time waste due to inactive CPUs.

In this work, the GNU parallel is applied in both lattice-based parameter space and LDS parameter space to obtain optimized parallel computing and to reduce the time cost for running all simulations. Specifically, several LIGGGHTS script files containing various parameter values are generated and assigned to the requested number of processors with the optimization from the GNU parallel, as shown in Figure 3.10.

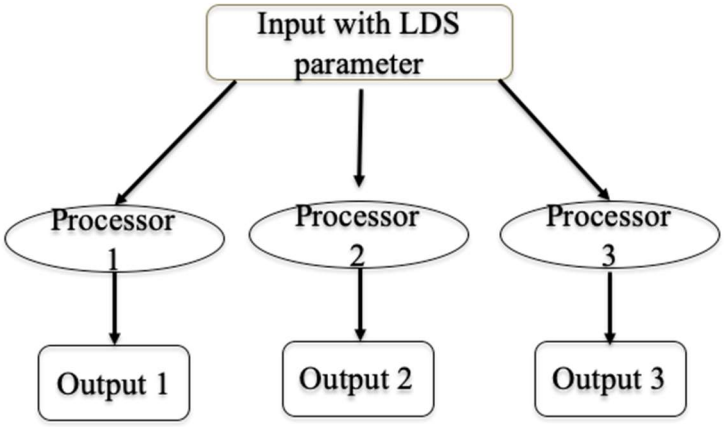

Figure 3.10 Task assignment of DEM simulation.

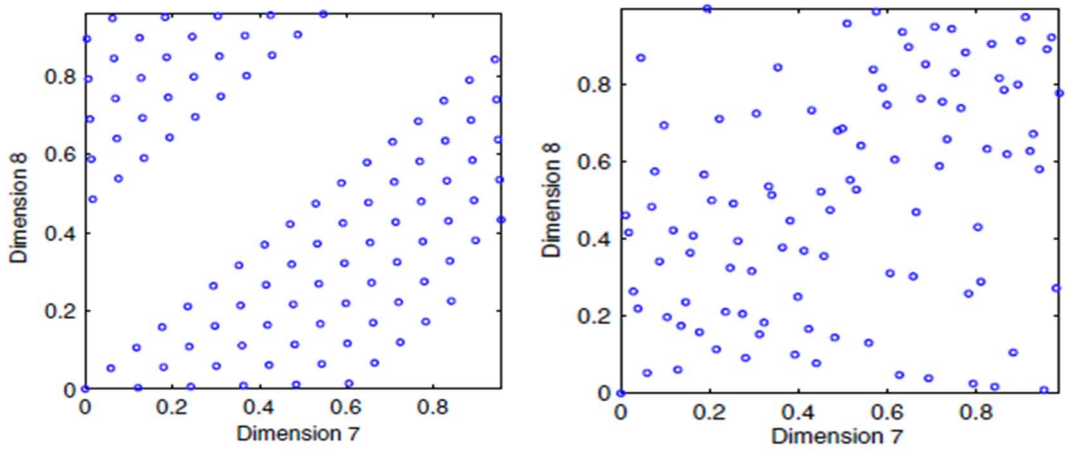

Figure 3.11 Data distribution of (a) Halton sequence (b) scrambled Halton sequence in 7th and 8th-dimensional system (Braaten & Weller, 1979).

Similarly, the parameter space is expanded for the LDS parameter sweep as well. However, instead of using equally-spaced values for each parameter, the LDS parameter sweep is generated as several mathematical sequences that are widely confirmed to have efficient parameter coverage (Schmid & Uhl, 2001; Kolenikov, 2012; Morokoff & Caflisch, 1994). However, each sequence may have various properties, and the choice of the sequence for generating the LDS parameter space can depend on the specific need of the research.

In this work, the scrambled Halton sequence, an evolution of the Halton sequence, is applied and is adjusted to the current parameter space. The sequences use coprime numbers as base numbers to generate points in the range [0, 1]. Compared with other sequences, the Halton sequence allows easier parameter addition for later work and avoid computational waste (Chunduri et al., 2018). Moreover, these sequences were shown to be effective in a lower-dimensional system (Kolenikov, 2012; Kocis & Whiten, 1997).

The only reason for choosing scrambled Halton sequence is, when it comes to a higher dimensional system, the Halton sequence presents a strong linear correlation between points that produce inefficient point distribution in high-dimensional space (Braaten & Weller, 1979). The scrambled Halton sequence introduces a permutation function to scramble the sequence to efficiently generate data points in a higher-dimensional system. Figure 3.11 shows 100 data distribution in the two sequences for a 7th and 8^{th}-dimension. A strong correlation of points can be observed in Figure 3.11 (a). Although 100 data points are insufficient for any parametric analysis, the linear correlation still exists, which makes scrambled Halton sequence more suitable to this work compared with the original Halton sequence.

Four parameters are studied in this work, generating a 4-dimensional parameter space. Since the scrambled Halton sequence only generates data points in the interval of 0 to 1, each parameter value has to be scaled to fit in the current parameter space, making it comparable with the lattice-based parameter sweep. The parameter value is scaled in such a way: Supposing the lower limit and the upper limit of the lattice-based parameter range are denoted by A and B, and the corresponding data point generated by the Scrambled Halton Sequence is X (0<X<1). Then, the scaled parameter value fit in [A, B] is$A + X(B - A)$.

Compared with the post-processing procedure in the first part of this parametric analysis, instead of investigating the velocity distribution of particles in front of the blade, a new post-processing area is defined for parameter sweep, and a new parameter is introduced to describe the performance of the particle spreading, which makes the result of the parameter sweep more visible and quantifiable.

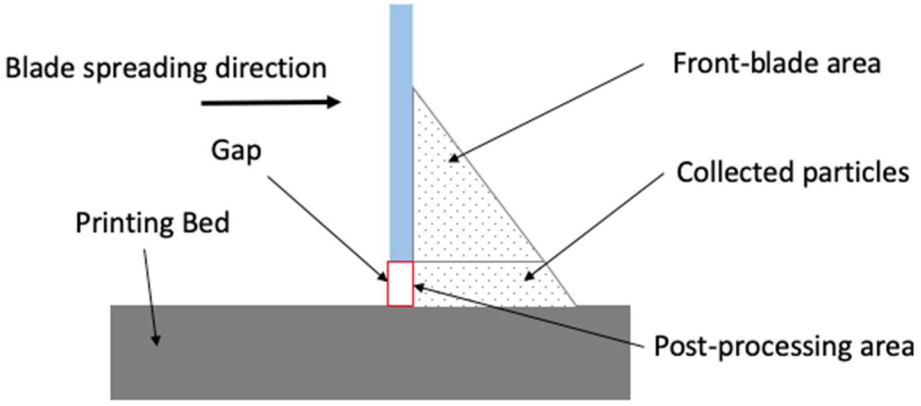

Figure 3.12 Post-processing area for parameter sweep.

In this parameter sweep section, instead of studying the area in front of the blade, a post-processing area under the blade is defined, as shown in Figure 3.12. The area is

defined as a rectangle with the same height as the current gap size of each simulation and the same width as the blade thickness. Besides, the depth of the post-processing area is the same as the blade width.

The newly defined parameter is called the mass flow rate, denoted by MFR. In general, it is a parameter describing how many particles are going through the gap. There is no doubt that a higher MFR should be expected in the particle spreading so that a higher manufacturing rate can be achieved. Based on some of the previous studies (Nan & Ghadiri, 2019; Chen et al. 2017), there are different ways to define the MFR, either by the particle volume or by the particle mass. In this work, mass-based MFR is adopted as the indicating parameter for the parameter sweep.

In each simulation, MFR can be calculated using Equation 15. To be specific, the mass of the ideal flow can be calculated by Equation 16, where w and h denote the width of the blade and the gap size correspondingly. ρ is the particle density, and v is the current blade speed. The mass of n particles under the blade is obtained using Equation 17, where m_i denotes the mass of i^{th} particle.

$$MFR = \frac{Mass\ of\ flow\ under\ blade}{Mass\ of\ ideal\ flow\ under\ blade} \tag{15}$$

$$Mass\ of\ ideal\ flow = w * h * v * \rho \tag{16}$$

$$Mass\ of\ flow = \sum_{i=1}^{n} m_i \tag{17}$$

Note that instead of using the thickness of the blade as the x-dimension of the post-processing area, the blade moving speed is adopted since the blade speed is a varying

parameter in this work, and the blade speed will have a certain influence on the flow behavior, which uses the same idea of the relative height from the first part of this work. By including the blade speed in the volume of the post-processing area, all cases are standardized and comparable with each other, and MFR can be considered as a transient parameter related to the blade motion.

MFR is used for checking the convergence of the parameter sweep. To describe each parameter space more comprehensively, mean, standard deviation, skewness, and kurtosis are calculated in each parameter space based on Equation 18 to Equation 21.

$$\text{Mean: } \bar{x} = \frac{\sum_{i=1}^{N} MFR_i}{N} \tag{18}$$

$$\text{Standard Deviation: S} = \sqrt{\frac{\sum_{i=1}^{N}(MFR_i - \bar{x})^2}{N}} \tag{19}$$

$$\text{Skewness: Skewness} = \frac{3 * (\bar{x} - median)}{S} \tag{20}$$

$$\text{Kurtosis: Kurtosis} = \frac{\sum_{i=1}^{N}(MFR_i - \bar{x})^4}{NS^4} \tag{21}$$

Here N denotes the total number of simulations included for current parameter space. The criterion is defined based on the relative change compared with the previous parameter space. The criterion for convergence is that the relative change of any one of the above statistical parameters in two continuous parameter space is within an acceptable range.

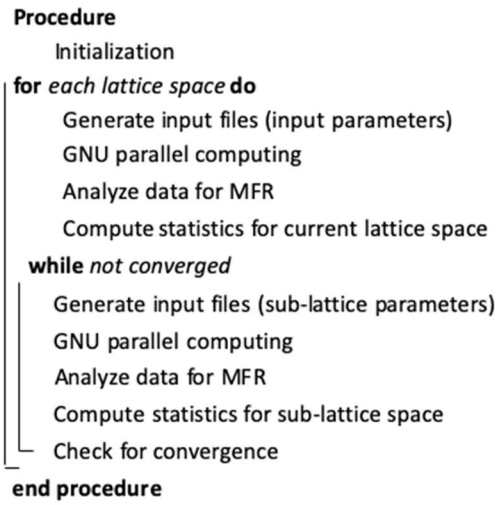

Figure 3.13 Lattice-based parameter space convergence checking algorithm.

The convergence analysis can be illustrated by a flowchart in Figure 3.13. In lattice-based parameter space, input files for DEM simulation are generated in certain sequences and are assigned to the processors running through GNU parallel computing, and independent simulation outputs are obtained. Then the data is processed to obtain MFR and further other statistical measures. For checking convergence, all statistics for current parameter space are compared with all statistics in sub-lattice obtained by following the same procedure. If it is not converged, a new lattice space is generated, and the procedure is repeated.

A key shortcoming of the lattice-based parameter sweep relates to convergence checking. The lattice parameter sweep algorithm does not permit efficient initialization or convergence check. For example, if the lattice size is too large, it may not describe the parameter space efficiently. If the meshing is too fine, the original parameter space may have already converged for a long time. Therefore, a significant computational effort is required for initialization and convergence estimation.

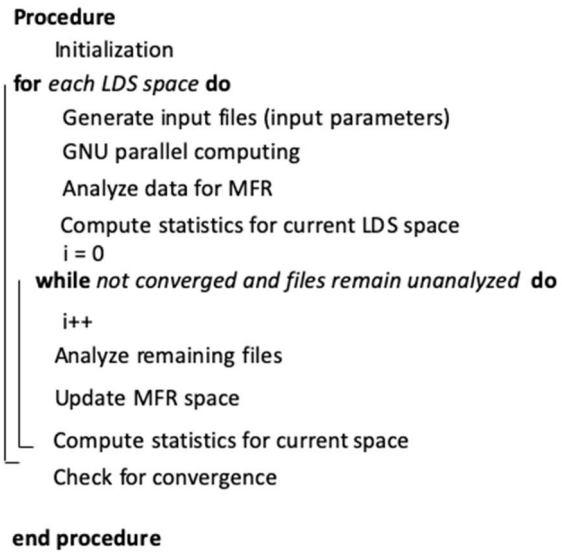

Figure 3.14 LDS parameter space convergence checking algorithm.

On the contrary, LDS convergence checking is an automatic procedure compared with the lattice-based parameter sweep. The convergence checking algorithm is described in Figure 3.14. Given a certain amount of input files for DEM simulations, all independent results are processed to get MFR for each parameter. Compared with a lattice-based sweep that is starting with the entire parameter space, LDS sweep starts with a small portion of data getting an MFR data source. All statistical measures are calculated at first and are compared as a base for the following LDS parameter space until the convergence criterion is reached.

The automation of LDS convergence checking lies in the generation of the new parameter space. Specifically, instead of generating a sub-lattice space with new parameters, LDS convergence checking generates a new parameter space based on the existing data by expanding the current parameter space step by step. Through this approach, the need for simulations for sub-lattice space is eliminated, and the influence of

improper selection on the first parameter space is more balanced than the lattice-based parameter sweep.

4. Results

In this chapter, the influence of the inter-particle friction, the particle size, the gap size, and the blade speed are analyzed and discussed at first. The effectiveness of the parameter sweep algorithm is validated in the latter part of this chapter.

4.1. Parametric Analysis in Particle Spreading

The dynamics of the particle spreading process is analyzed using the velocity distribution along with different layers on the printing bed. Although simulations are different from each other with various parameter values, the differences are not at a scale that can be captured through visualization. An example simulation in Figure 4.1 can directly demonstrate the particle behavior and the interaction between particles and the blade. The entire simulation is animated by linking a certain number of continuous snapshots based on the timestep.

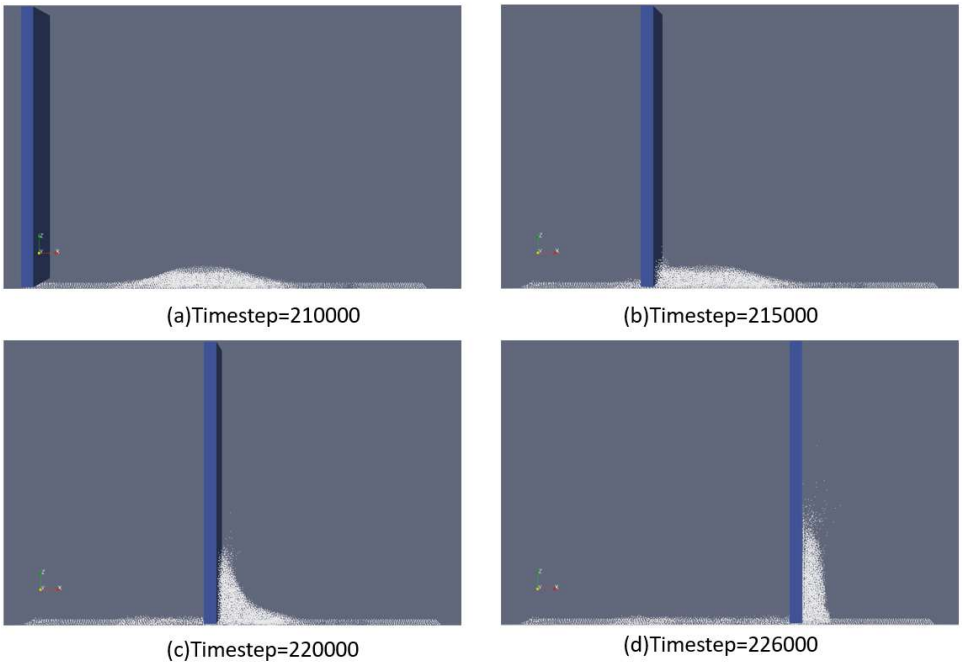

Figure 4.1 Particle behavior during DEM simulation.

Despite macroscopic similarities in the visualization of particle behavior, the particle velocity distribution can vary greatly with different parameter values. To further elucidate the ideal velocity distribution, two example curves from the later analysis are given in Figure 4.2. A smooth increase in v_x in different layers, as shown in Figure 4.2 (a), can be considered as an ideal flow, which is observed from visualization, providing a higher particle spreading quality with an even layer of particles distributed on the printing bed. Such an ideal flow is clearly differentiated from the flow of a uniform v_x distribution, as shown in Figure 4.2 (b), whose visualization is shown in Figure 4.2 (d).

Two typical undesired v_x distributions are presented Figure 4.2 (b) and (c). One is the uniform distribution corresponding to an inefficient spreading resulted from, e.g., a large gap with small particles. From the visualization, the blade moves towards the surface of the particle pile, and clogging is found at the blade tip, as shown in Figure 4.2 (e), leading to an uneven distribution of particles. In reality, such an uneven distribution requires varying levels of energy in the particle bonding during sintering, which can create voids and pores in the final product (Han et al., 2019). Another possible reason for such a uniform v_x distribution may come from the high blade speed. A similar observation is also presented in previous work (Nan et al., 2018). Figure 4.2 (c) and (f) show another kind of undesired v_x distribution. This highly fluctuating v_x distribution results in a messy and unstable particle flow and may lead to defects in the final product.

Note that Sections 4.2-4.5 consider uniform particle size distribution. While particle sizes can vary within a given sample, the uniform particle size is utilized in the initial analysis to understand the effect of various parameters. In Section 4.6, the effect of particle size variation is considered by using Weibull distribution, as discussed in chapter.

In addition, to study the influence of the restitution coefficient, simulations include five different values listed in Table 3.1 are conducted. The result suggests a neglectable effect on the flow behavior.

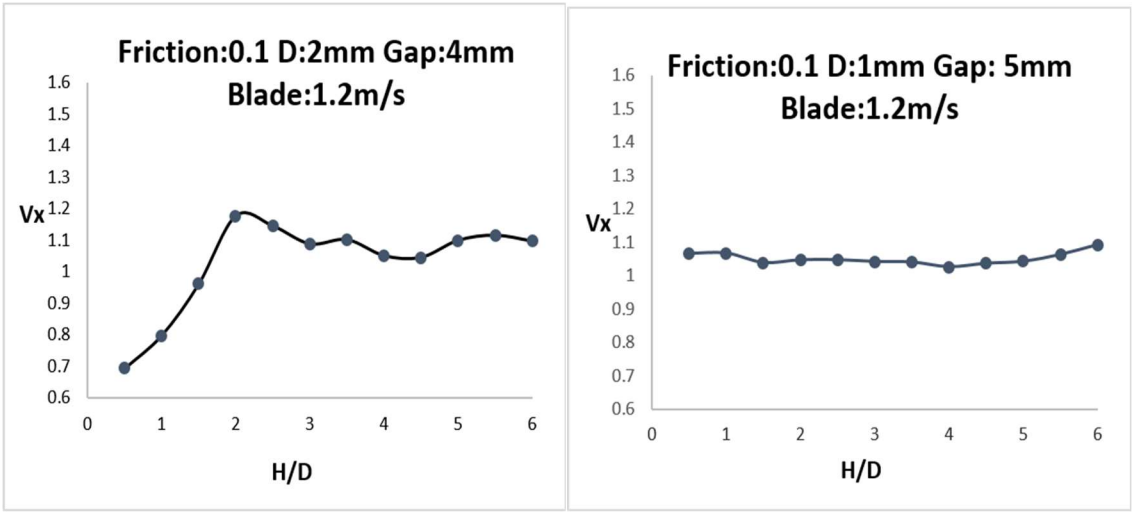

(a) (b)

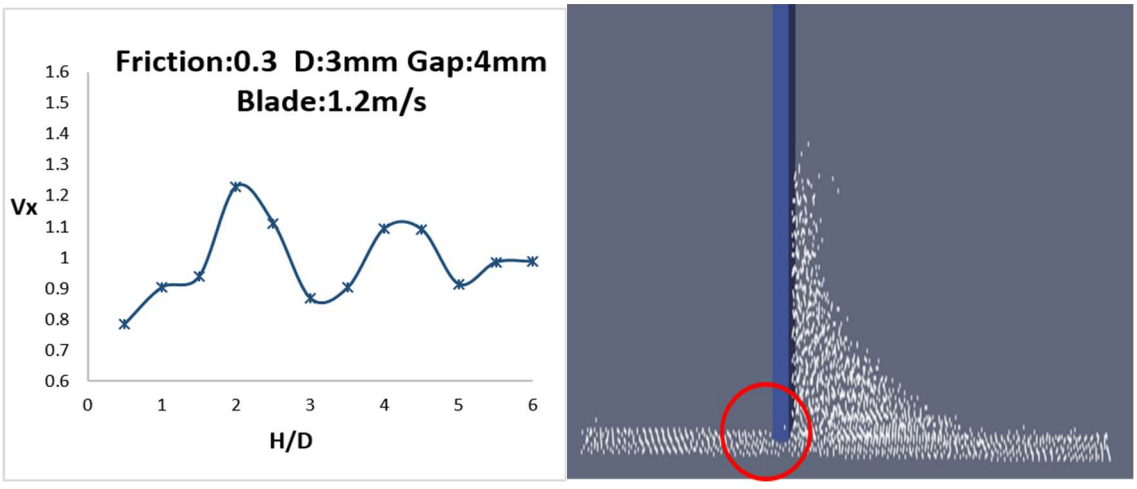

(c) (d)

Figure 4.2 Examples of v_x distribution and visualization for (a)(d) ideal spreading (b)(e) inefficient spreading (c)(f) unstable spreading.

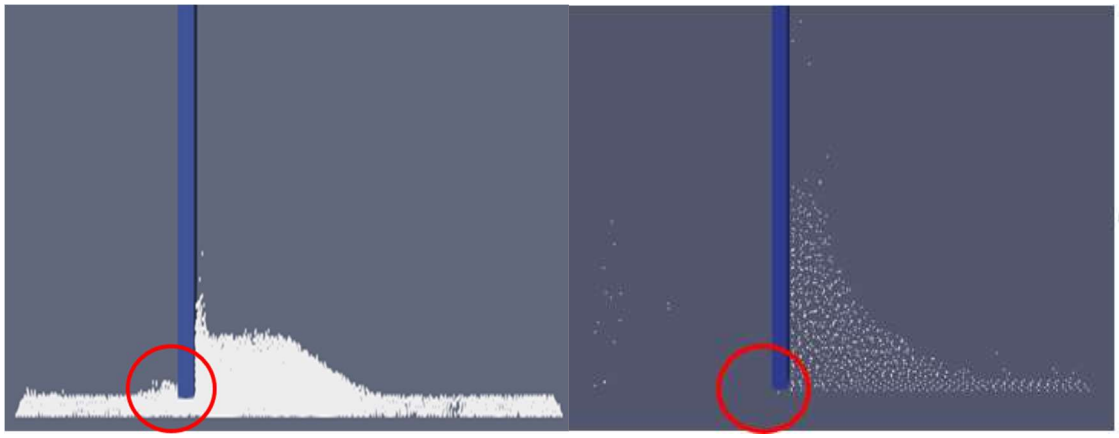

(e) (f)

Figure 4.2 Examples of v_x distribution and visualization for (a)(d) ideal spreading (b)(e) inefficient spreading (c)(f) unstable spreading.

4.2. The Effect of Particle Size

Firstly, the effect of the particle size is analyzed. In this analysis, all four parameters (particle size, friction, gap size, and blade speed, parameter values listed in table 3.1) are compared to understand the effect of particle size in the parameter space, and some correlation between parameters are considered. Such comparison is employed to later analysis part as well.

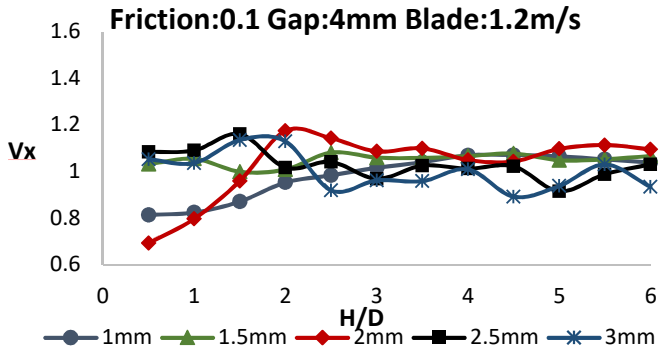

(a)

Figure 4.3 Different particle size with friction of (a) 0.1 (b) 0.2 (c) 0.3.

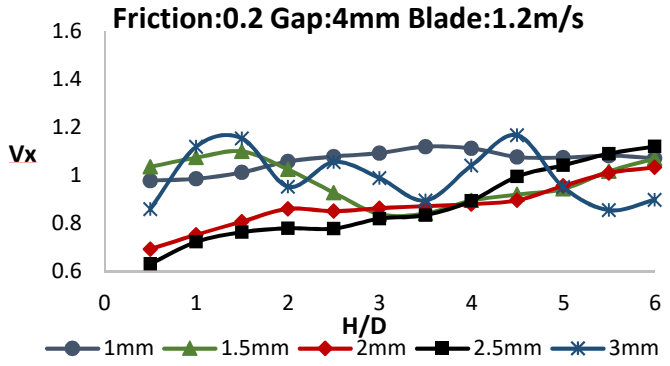

(b)

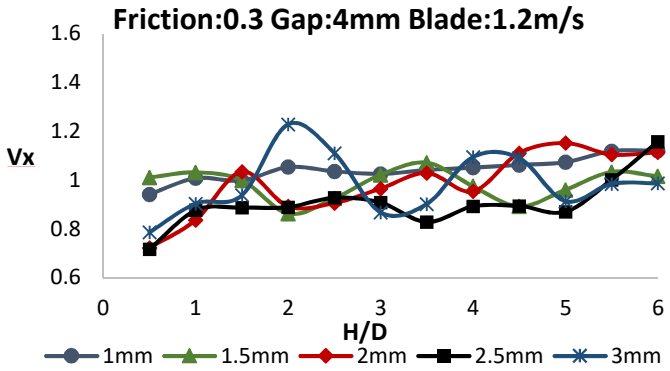

(c)

Figure 4.3 Different particle size with friction of (a) 0.1 (b) 0.2 (c) 0.3.

Comparing the curves at low friction in Figure 4.3 (a), it can be observed that smaller particles tend to have a smoother v_x distribution among layers (e.g., 2mm). Larger particles (2.5mm & 3mm) tend to have higher velocity fluctuations. Smaller particle sizes, including 1mm and 1.5mm particles, tend to have uniform velocity distribution, which can be explained by the large gap from the visualization and can be verified in the later gap size analysis (Section 4.3). Comparing the three plots, it can be noted that increasing the friction does have some influence on small particles (e.g., 2mm particle),

but it does not change the overall trend. The effect of particle size is more dominant than the effect of the friction, which can be verified in the friction analysis (Section 4.5).

The variation of the blade speed with particle size is shown in Figure 4.4. Middle-sized particles tend to have smoother velocity distribution (e.g., 2mm and 2.5 mm in Figure 4.4 (a)). A similar result is observed in previous analyses with various inter-particle friction. The reason for this behavior can be concluded from the relative size of gap and particle diameter, which will be further verified in Section 4.3.

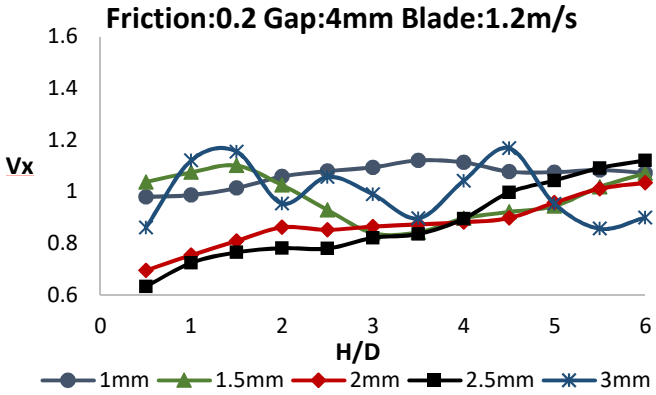

(a)

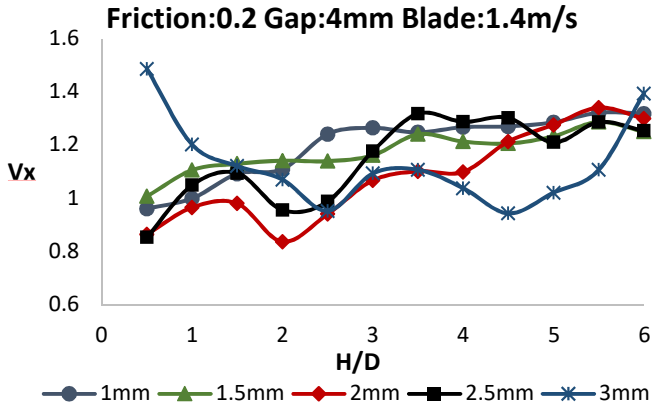

(b)

Figure 4.4 Different particle size with blade speed of (a) 1.2 (b) 1.4 (c) 1.6 m/s.

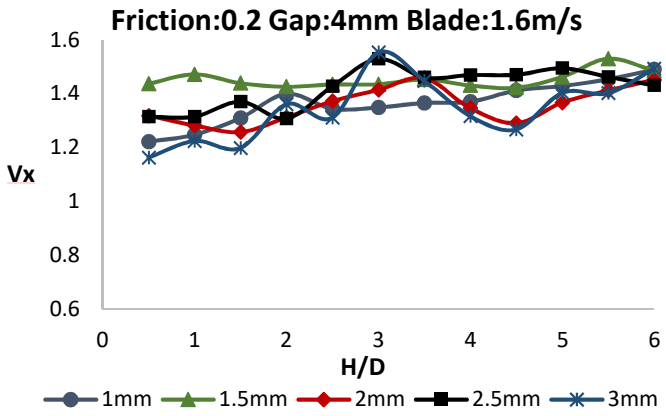

(c)

Figure 4.4 Different particle size with blade speed of (a) 1.2 (b) 1.4 (c) 1.6 m/s.

The particle velocity distribution is more uniform at higher blade speed, as shown in Figure 4.4 (c). As mentioned before, such particle behavior may due to the fact that all layers of particles tend to move with the blade instead of going through the gap, which is unwanted and produces inefficient spreading flow.

The variation of particle size with different gap sizes is shown in Figure 4.5. The velocity distribution of larger particles can fluctuate (e.g., 3mm particles in Figure 4.5 (c)). The velocity distribution of smaller particles can be either fluctuating or uniform depending on the gap size for the corresponding particle size. Comparing the three plots in Figure 4.5, the trends are not very clear because, in some cases, the gap is equal to or smaller than particle diameter (e.g., in Figure 4.5 (a) and some cases in Figure 4.5 (c)). The data in these unrealistic cases are plotted only for consistency in the lattice parameter space. When the gap is 3mm, 1.5mm particles can create ideal flow compared with others, and this double sizing relation is exactly the same as before when the gap is 4mm with 2mm particles. This observation indicates that only a perfect match of the gap size

and the particle size can create ideal flows. Such perfect matching was also observed in a previous study (Nan & Ghadiri, 2019). However, such a relationship is not very clear in Figure 4.5 (c), when the gap is 5mm with 2.5mm particles. Therefore, it is surmised that the generation of an ideal flow not only depends on the particle size matching with the gap but also depends on the particle size itself. In other words, the particle size is more significant than the gap size in determining the particle spreading.

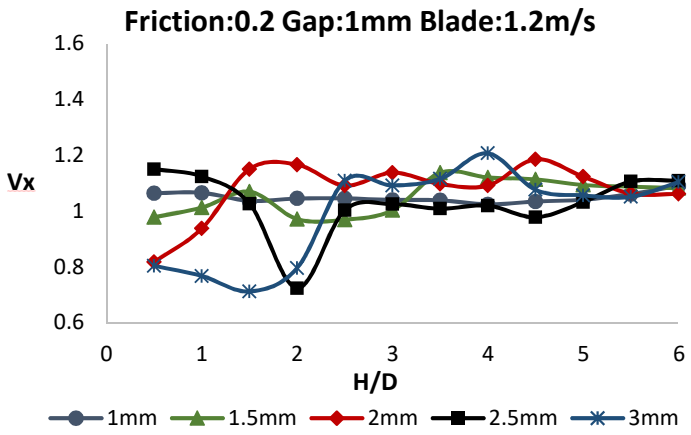

(a)

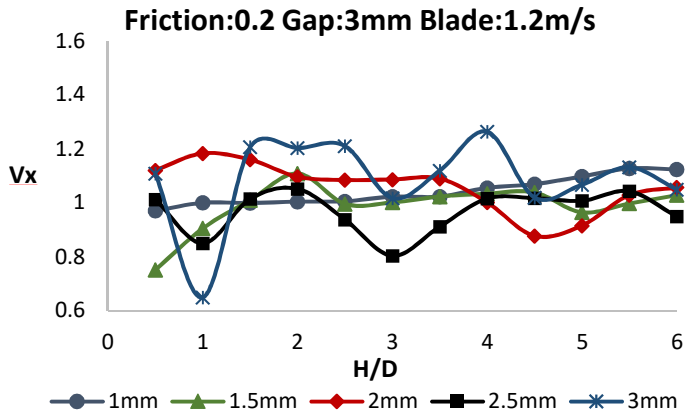

(b)

Figure 4.5 Different particle size with gap size of (a) 1 (b) 3 (c) 5 mm.

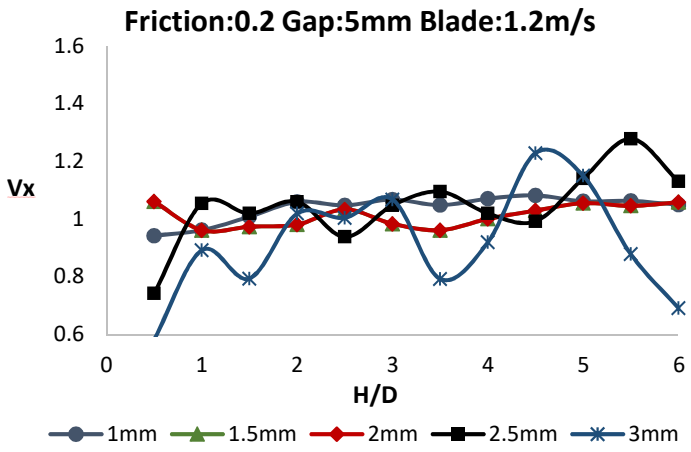

(c)

Figure 4.5 Different particle size with gap size of (a) 1 (b) 3 (c) 5 mm.

4.3. The Effect of Gap Size

As indicated in the previous analysis, a size matching between the particle and the gap can produce a more ideal flow. Therefore, the effect of the gap size is analyzed next.

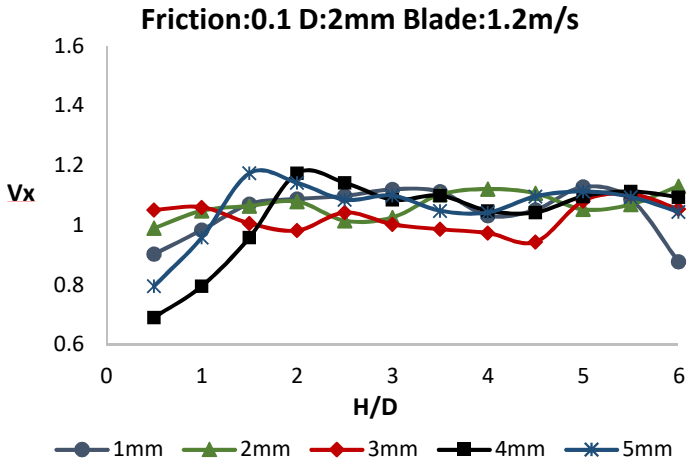

(a)

Figure 4.6 Different gap size with friction of (a) 0.1 (b) 0.2 (c) 0.3.

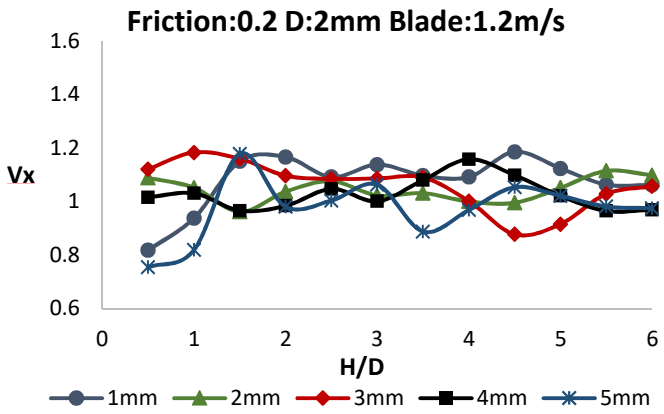

(b)

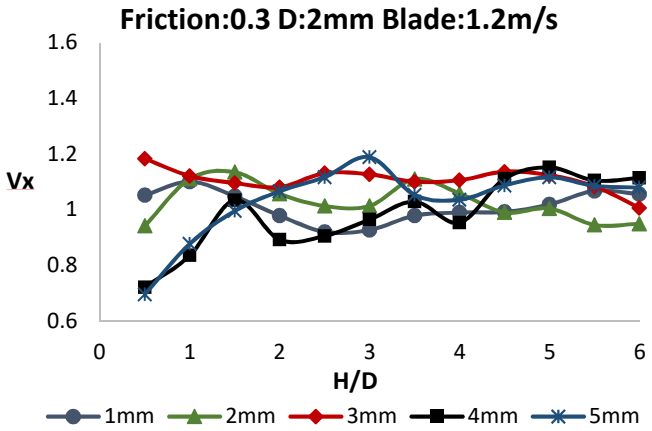

(c)

Figure 4.6 Different gap size with friction of (a) 0.1 (b) 0.2 (c) 0.3.

The effect of friction vs. gap size is shown in Figure 4.6. It has been noted earlier that a gap size that is double the particle size produces good flow characteristics. Comparing the low friction simulations shown in Figure 4.6 (a), this double sizing relation still exists. Due to the selection of current particle diameter and the gap size, other cases in Figure 4.6 (a) are considered result in inefficient spreading. Similar to the observation in

the particle size analysis, comparing Figure 4.6 (a), (b), and (c), increasing friction doesn't change the overall trend of each curve much. However, higher friction can create more fluctuation even for the ideal 2mm particle and 4mm gap, which reduces the overall spreading quality.

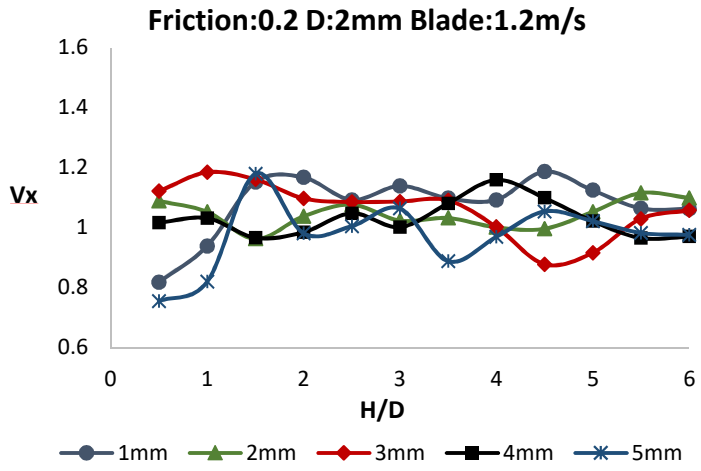

(a)

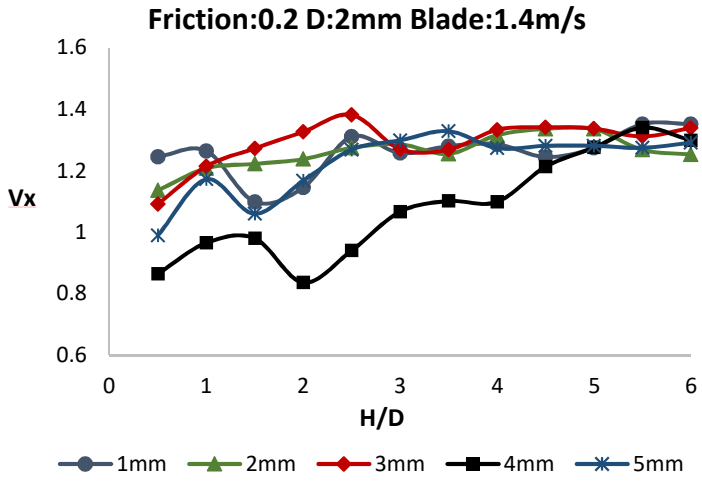

(b)

Figure 4.7 Different gap size with blade speed of (a) 1.2 (b) 1.4 (c) 1.6 m/s.

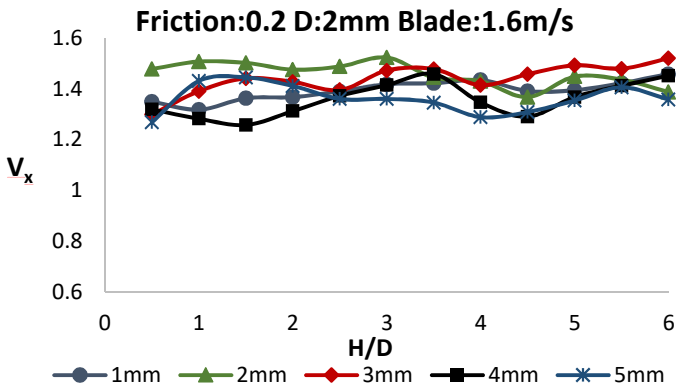

(c)

Figure 4.7 Different gap size with blade speed of(a) 1.2 (b) 1.4 (c) 1.6m/s.

Figure 4.7 shows the analysis of blade speed and the gap size. The trend for each gap size does not change much by varying the blade speed. In higher blade speed cases shown in Figure 4.7 (c), the curves are compressed but are similar to lower blade speed cases. Therefore, the blade speed can be considered to have some effect on the flow behavior, but the gap size has a more significant effect. A higher blade speed tends to produce a uniform velocity distribution indicating particles' tendency to move with the blade rather than going through the gap, which produces an unstable spreading. A similar effect of high-speed can also be observed in later analysis for the effect of the blade speed in Section 4.4.

Figure 4.8 compares different gap sizes and particle sizes. As noted earlier, Figure 4.8 (a) shows that if the gap is around two times the particle diameter, a smooth velocity distribution is observed (e.g., 2mm gap with 1mm particles).

Comparing Figure 4.8 (a) (b) (c), the particle size is considered to have a stronger effect on the flow behavior because of the fact that, for larger particles, even though the gap is twice the size for the current particle diameter, velocity can still fluctuate layer by layer. This indicates that the particle size is a dominant factor. As reflected in the previous particle diameter analysis, smaller particles tend to produce an ideal flow.

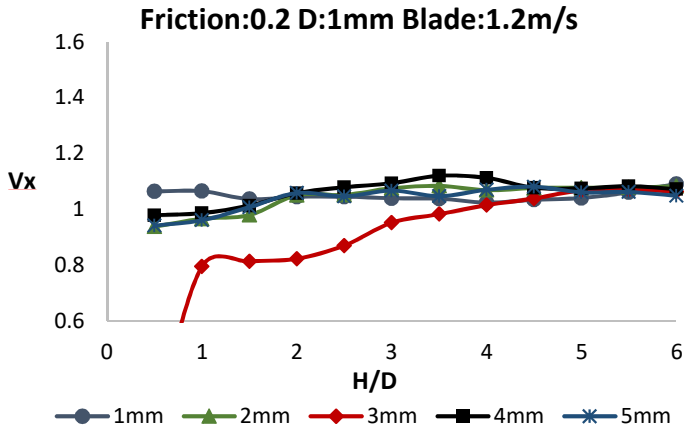

(a)

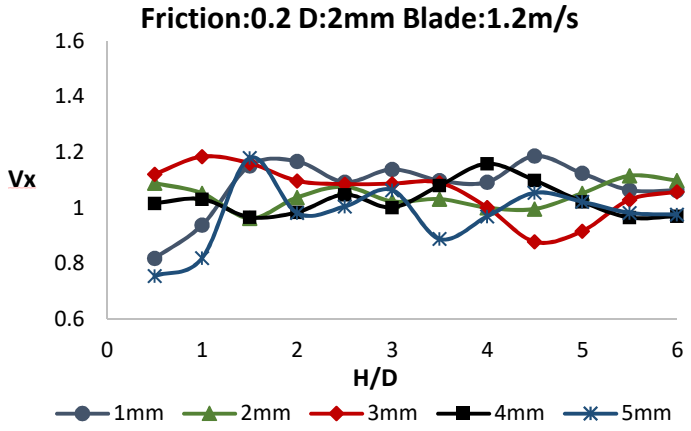

(b)

Figure 4.8 Different gap size with particle size of (a) 1 (b) 2 (c) 3 mm.

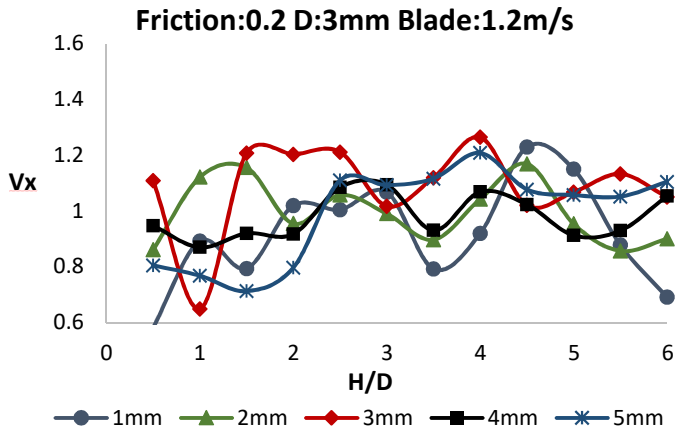

(c)

Figure 4.8 Different gap size with particle size of (a)1 (b)2 (c)3 mm.

4.4. The Effect of Blade Speed

Generally, a higher blade speed produces a uniform velocity distribution resulting in an inefficient spreading flow. In this section, the effect of the blade speed is analyzed in detail.

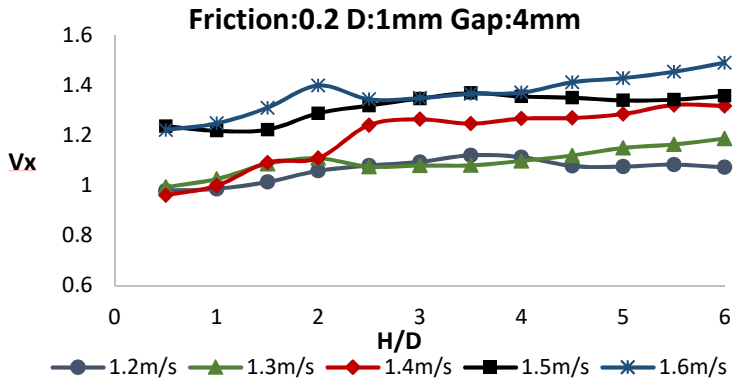

(a)

Figure 4.9 Different blade speed with particle size of (a) 1 (b) 2 (c) 3 mm.

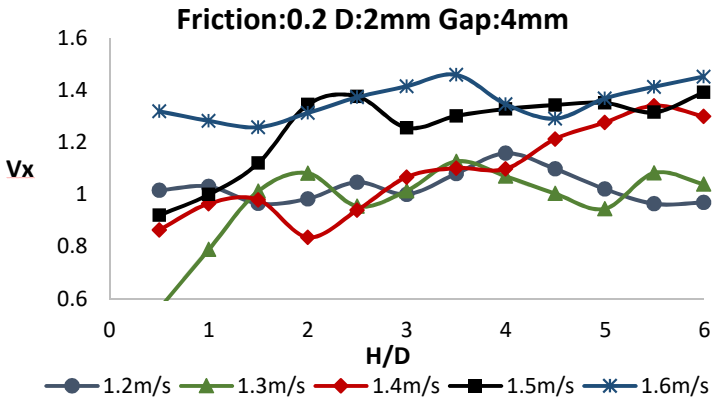

(b)

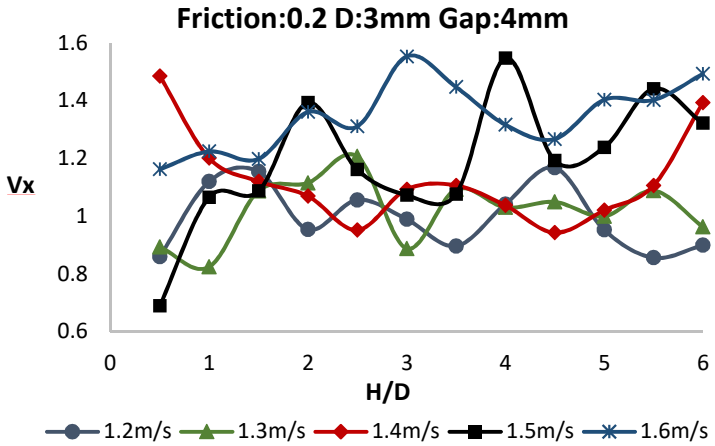

(c)

Figure 4.9 Different blade speed with particle size of (a) 1 (b) 2 (c) 3 mm.

Figure 4.9 shows that blade speed is the upper-limiting speed at which particles can move. This observation shows the effectiveness of the DEM simulation setup in this work. In reality, the velocity of particles should not be greater than the blade speed because the 'bouncing' effect of particles given by the blade should be minimized to guarantee an efficient flow through the gap. Despite that, the interaction between

particles and the blade is automatically defined as rigid in simulations. Figure 4.9 shows that rigid interaction does not produce unrealistic flow behavior.

Comparing Figure 4.9 (a) (b) (c), varying the particle size does change the trends. Again, it is found that the particle size has a more dominant effect than the blade speed.

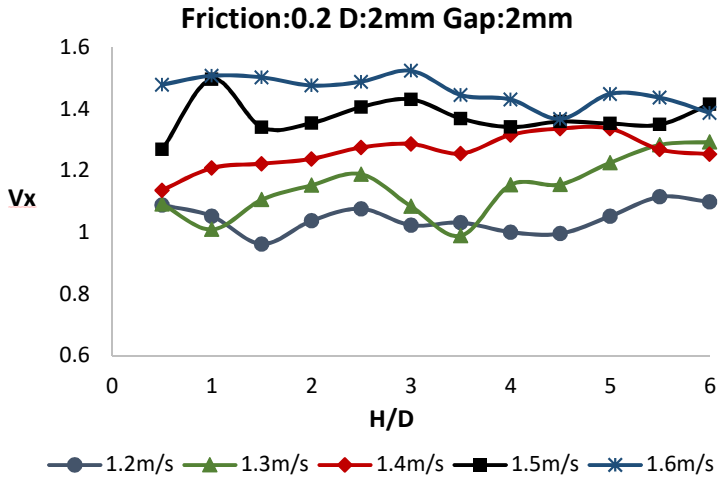

(a)

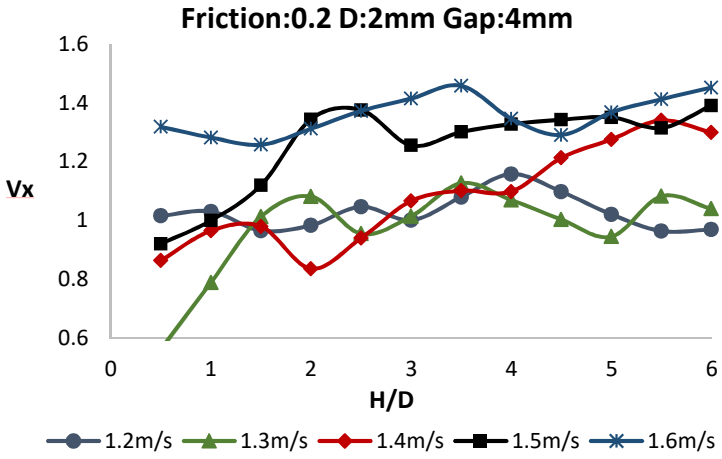

(b)

Figure 4.10 Different blade speed with gap size of (a) 2 (b) 4 (c) 5 mm.

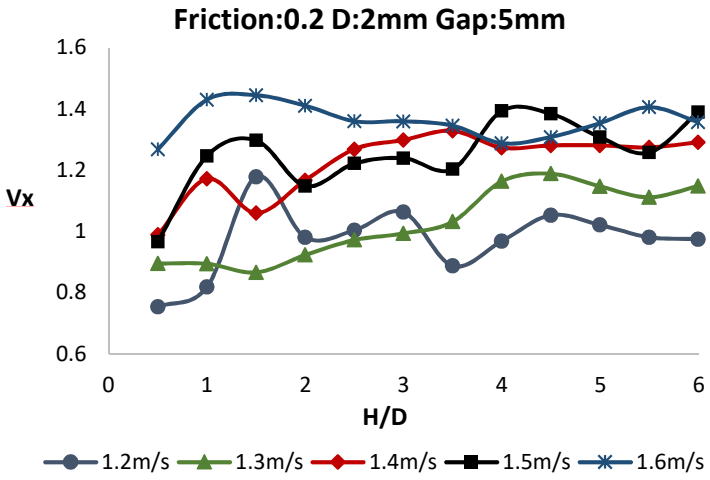

(c)

Figure 4.10 Different blade speed with gap size of (a) 2 (b) 4 (c) 5 mm.

The effect of blade speed vs. the gap size is shown in Figure 4.10. Varying the gap size can lead to changes in particle movement. Results indicate that the gap size is more dominant than the blade speed.

Larger gap sizes in Figure 4.10 (c) do not produce smooth spreading. However, a simulation with the same particle size and gap size but with a lower friction coefficient of 0.1 produces a smooth flow, as shown in Figure 4.6 (a). Therefore, the absence of a smooth curve here is due to the interaction of higher friction coefficient with other parameters. Although the result is not very clear for current parameter space, considering the blade speed effect from other analysis parts, a lower blade speed tends to produce smooth flow if other parameters are ideal.

The effect of the blade speed vs. the friction is shown in Figure 4.11. Higher friction increases the maximum velocity that particles can reach (e.g. 1.6m/s in Figure 4.11

(a)(b)(c)). Varying friction doesn't change curve trends very much. Therefore, friction is considered to be less dominant compared with the gap size in influencing spreading.

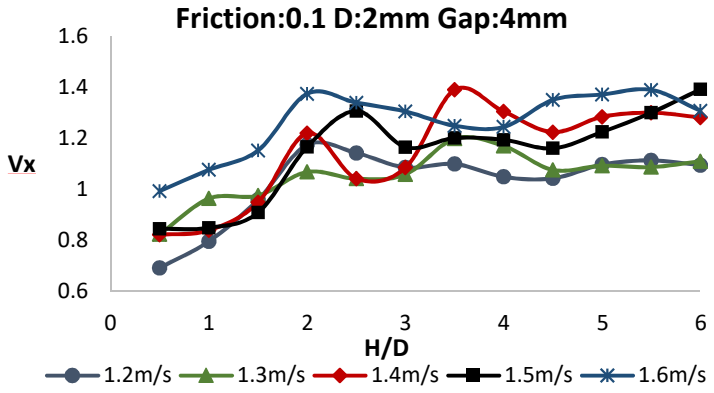

(a)

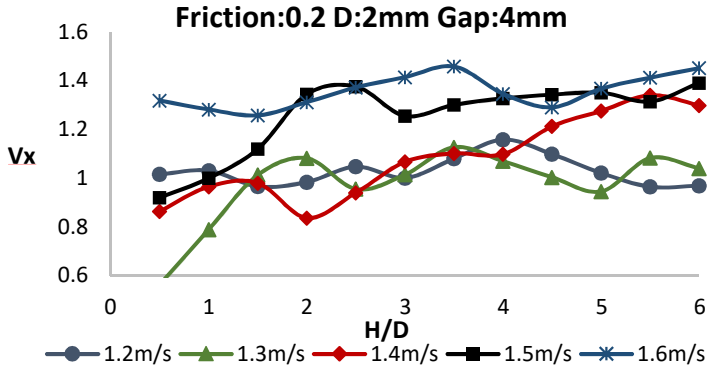

(b)

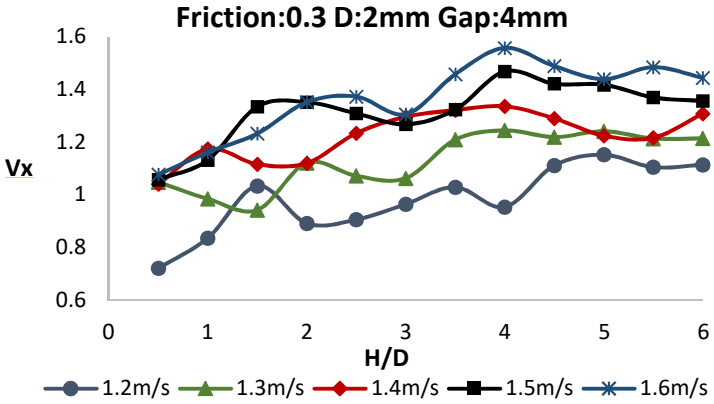

(c)

Figure 4.11 Different blade speed with friction of (a) 0.1 (b) 0.2 (c) 0.3.

4.5. The Effect of Inter-particle Friction

Figure 4.12 analyzes the interaction between blade speed and friction coefficient. The lower friction coefficient and low blade speed tend to produce a smoother flow (e.g., friction 0.1 and 0.15 in Figure 4.12 (a)). Increasing the blade speed makes the velocity distribution more uniform, which is the same as the observation in Section 4.4 and is undesired. Higher friction case (0.3) is especially sensitive to the higher speed, as the shape variation indicated in Figure 4.12 (a) and (c).

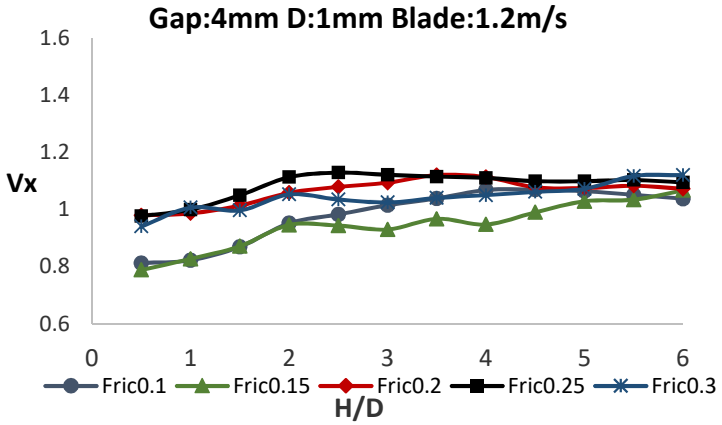

(a)

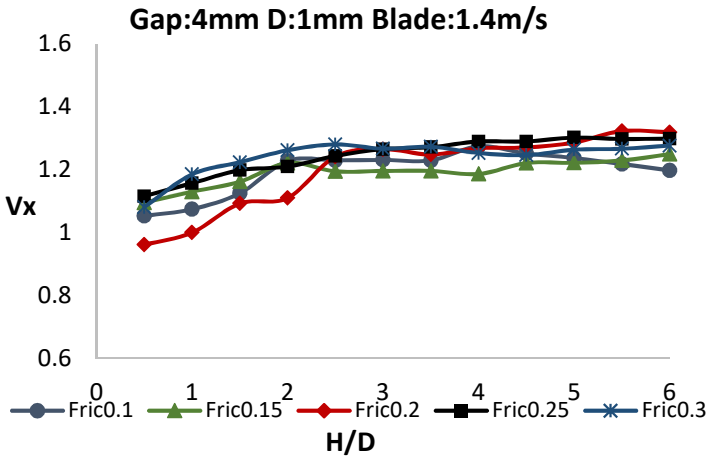

(b)

Figure 4.12 Different friction with blade speed of (a) 1.2 (b) 1.4 (c) 1.6 m/s.

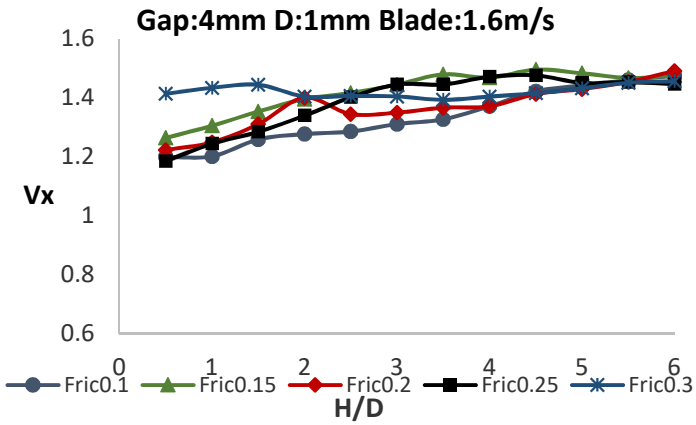

(c)

Figure 4.12 Different friction with blade speed of (a) 1.2 (b) 1.4 (c) 1.6 m/s.

As for the friction vs. the gap size described in Figure 4.13, the friction has a limited effect on the spreading process compared with the gap size because increasing the gap size has a great effect on the curve trends in Figure 4.13 (a) (b) and (c). Note that the effect of the gap size is found to be greater than that of the blade speed in Section 4.1.2. Here, it is found that the effect of the blade speed is greater than friction.

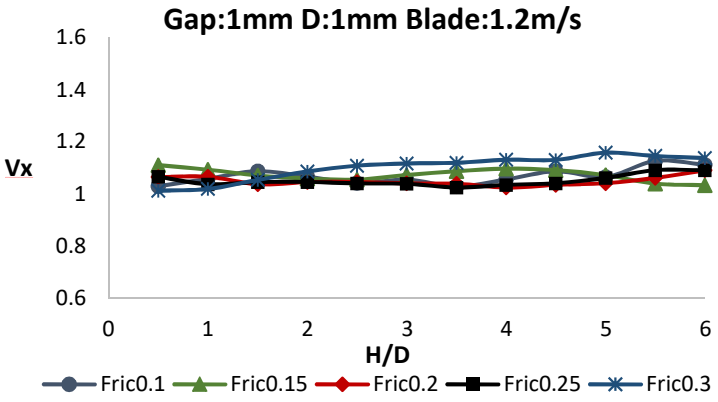

(a)

Figure 4.13 Different friction with gap size of (a) 1 (b) 3 (c) 4 mm.

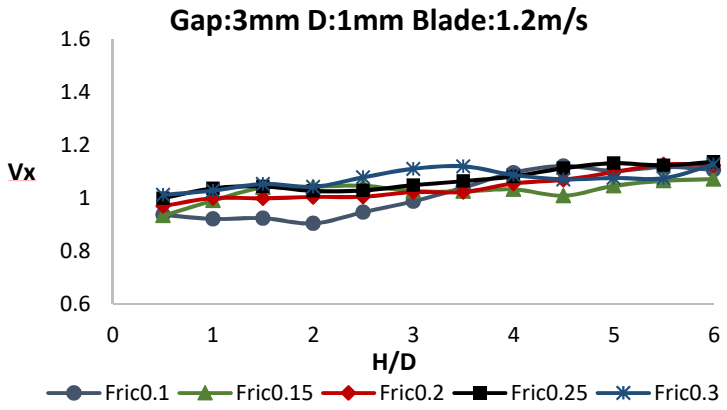

(b)

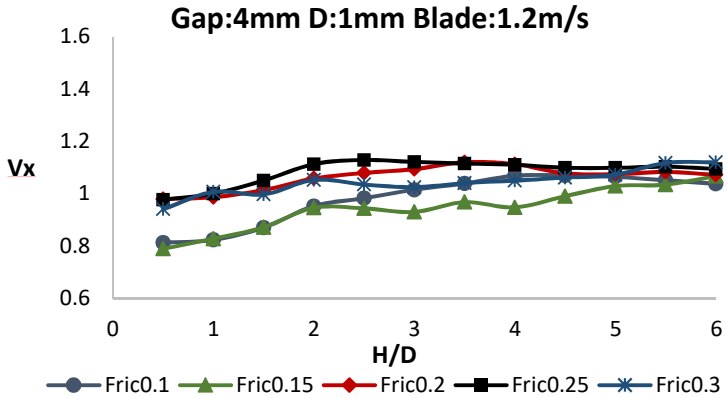

(c)

Figure 4.13 Different friction with gap size of (a) 1 (b) 3 (c) 4 mm.

The analysis of the particle size vs. friction is shown in Figure 4.14. Small particles with lower friction tend to produce a smoother curve (e.g., Friction 0.1 in Figure 4.14(a)), though it is not clear due to the larger gap size for 1mm particles. Increasing the particle size creates fluctuation even when the friction is in a lower range. In such a case, the particle size is a more dominant factor in determining the spreading quality.

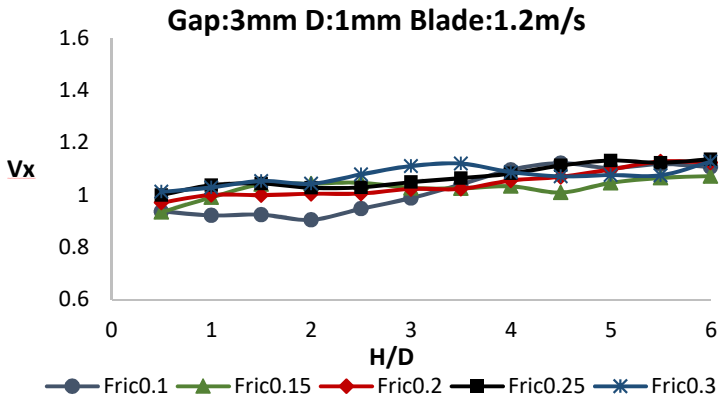

(a)

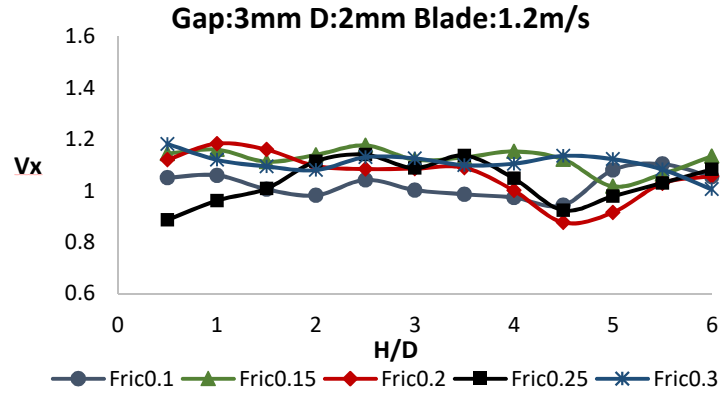

(b)

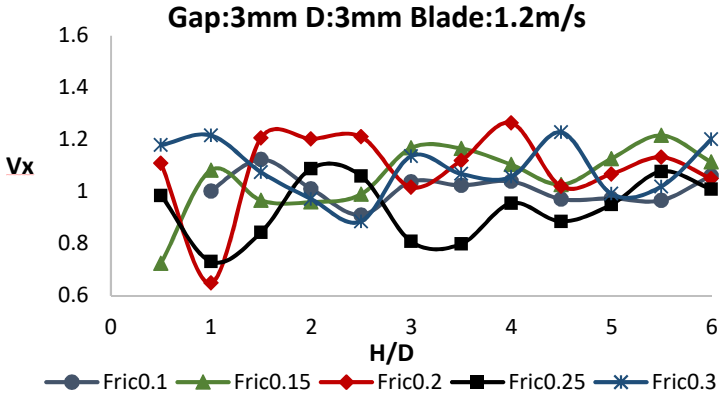

(c)

Figure 4.14 Different friction with particle size of (a) 1 (b) 2 (c) 3 mm.

4.6. The Effect of Particle Size Distribution

The particle size distribution is investigated using a Weibull distribution, as described in Chapter 3. Two particle size ranges are considered to investigate the effect of powder quality. The same simulation setup is used with varying particle sizes in this section. Two particle size distributions are described and are referred to as narrow distribution and wide distribution in the following analysis. The morphology of the two distributions can be described by an example of the 2 mm mean particle size case shown in Figure 4.15. Simulations with varying mean particle size are analyzed in this section.

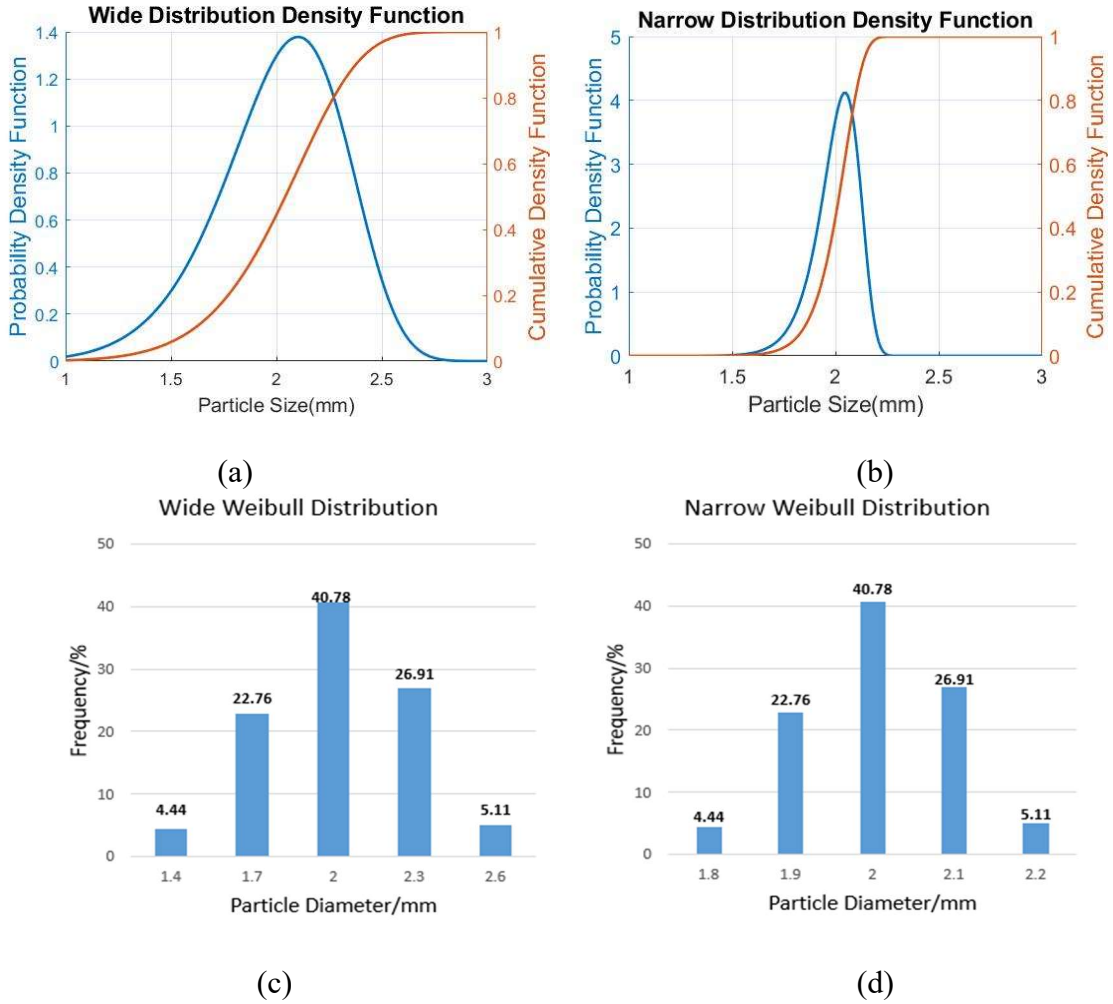

Figure 4.15 Two types of particles with (a)(c) wide (b)(d) narrow Weibull distribution.

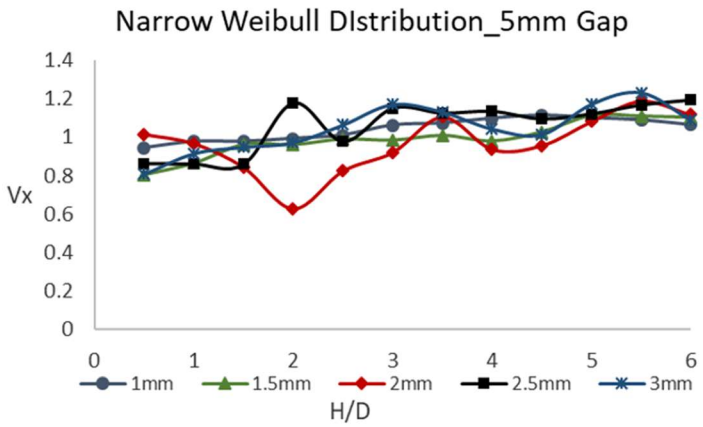

(a)

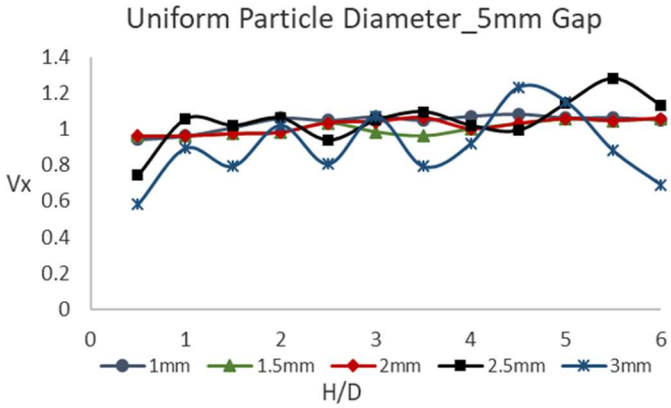

(b)

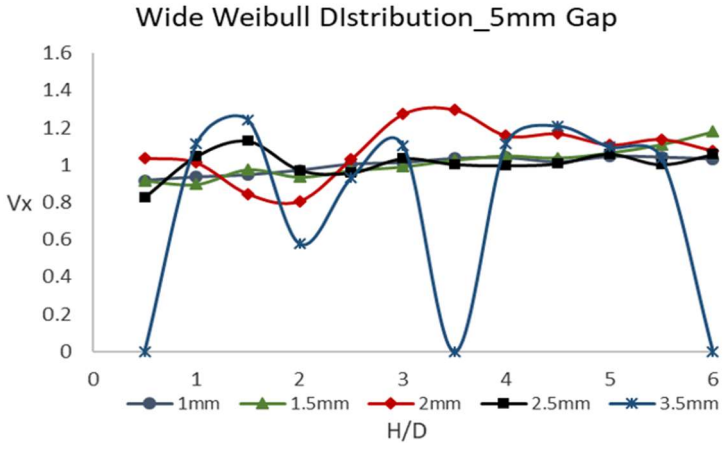

(c)

Figure 4.16 v_x distribution of particles with (a) narrow (b) uniform (c) wide distribution under 5mm gap.

To further investigate the effect of each parameter, each case of narrow distribution and a uniform distribution is presented correspondingly in Figure 4.17. It is observed that 1mm and 1.5mm cases do not show desired spreading characteristics due to the small particle diameters and the relatively large gap. This trend continues for 2mm mean particle diameter, as shown in Figure 4.17 (c). The spreading characteristics for 2.5mm and 3mm mean diameter cases are improved, as shown in Figure 4.17 (d) and (e).

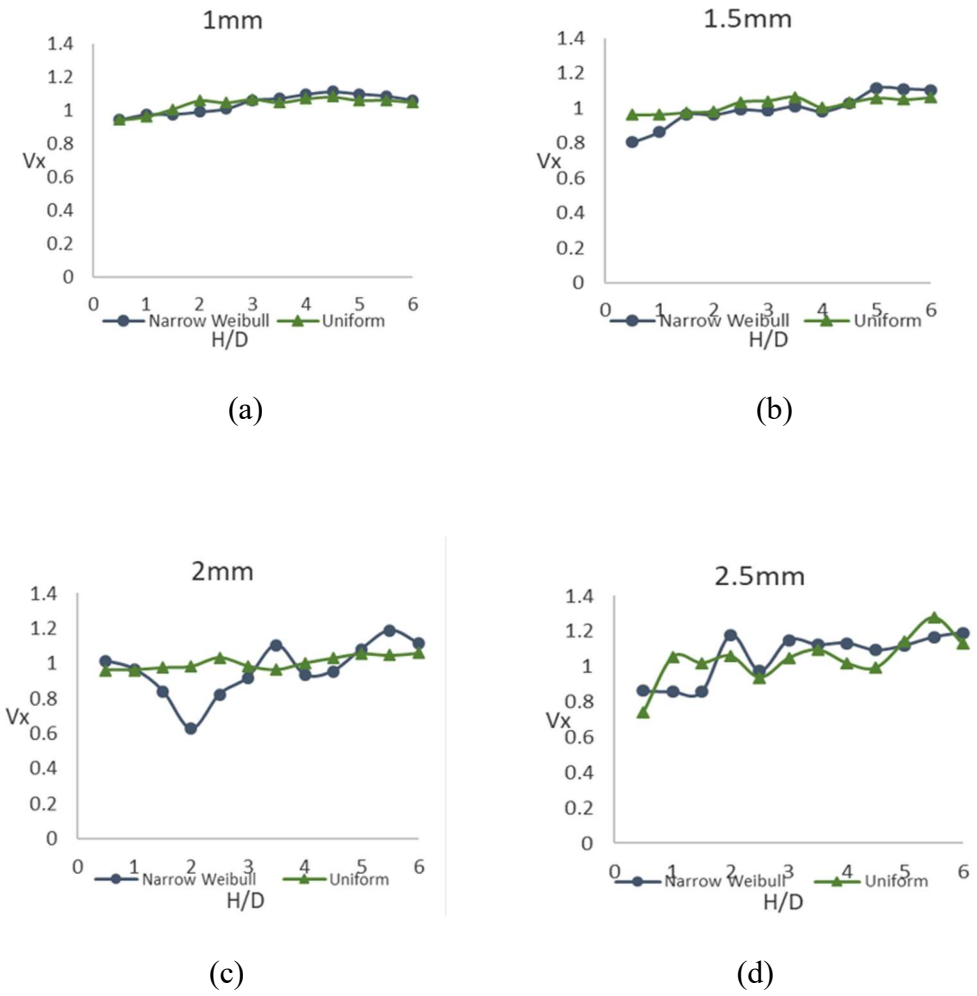

Figure 4.17 Comparison of v_x for narrow and uniform distribution of (a) 1 (b) 1.5 (c) 2 (d) 2.5 (e) 3 mm particles.

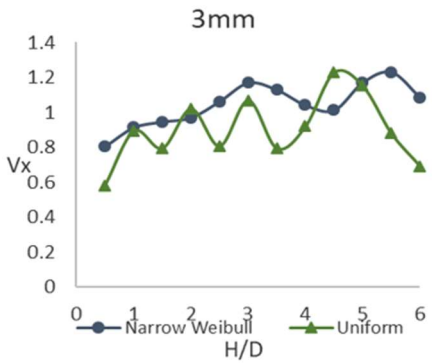

(e)

Figure 4.17 Comparison of v_x for narrow and uniform distribution of (a) 1 (b) 1.5 (c) 2 (d) 2.5 (e) 3 mm particles.

The results for the two particle size distributions but with varying gap sizes are shown in Figure 4.18. The first observation of trend for each case in Figure 4.18 (a) has confirmed the analysis in Section 4.2 that smaller particles with an optimum gap tend to produce a better flow. Even though the fluctuation exists in the 2.5mm case, the overall flow quality is still acceptable. Comparing Figure 4.18 (a) and Figure 4.16 (a) with the same narrow particle size distribution but with a fixed 5mm gap, the spreading characteristics of the 2mm case are improved, which evidenced the previous guess that the unclear flow behavior is due to the improper gap size. Additionally, such improvement of the spreading characteristics for larger particles is greater than smaller particles, based on the observation that 1mm and 1.5mm cases have not much difference when changing the gap size comparing Figure 4.18 (a) and (b).

As shown in Figure 4.18 (c), even the wide Weibull distribution tends to produce a uniform velocity distribution with an optimum gap. In these cases, most particles tend to move with the blade. In conclusion, with a proper selection of the gap, both a narrow

Weibull distribution and uniform distribution can improve the spreading characteristics if particles are small.

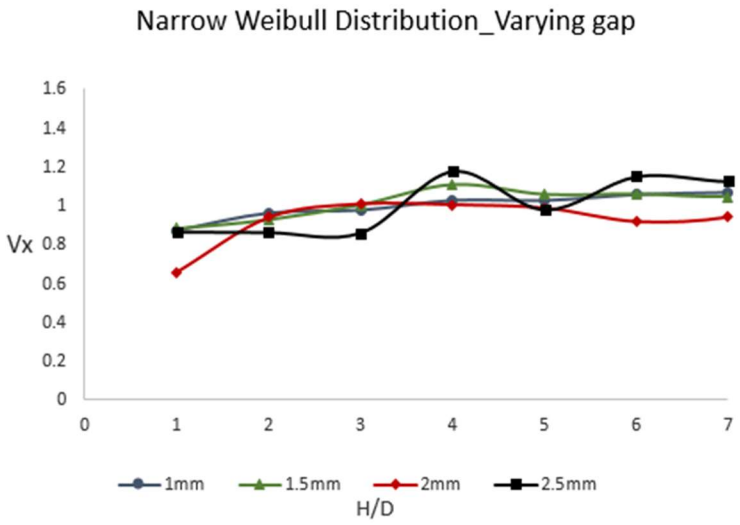

(a)

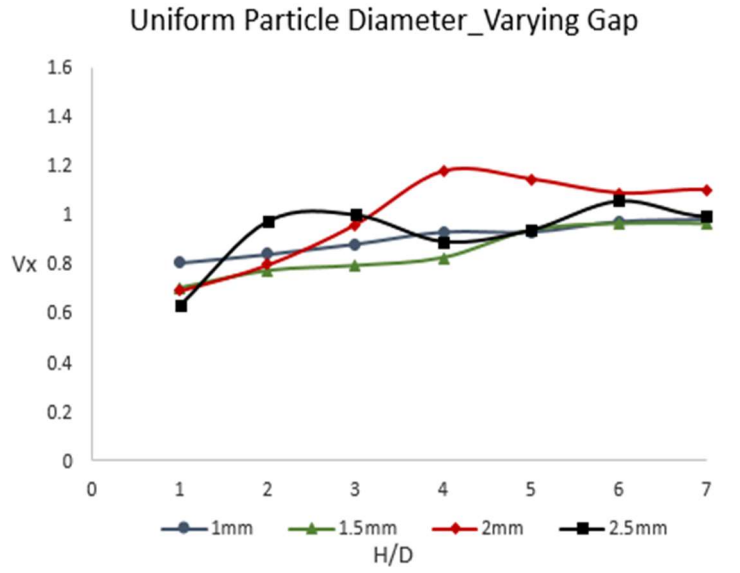

(b)

Figure 4.18 v_x distribution of particles with (a) narrow (b) uniform (c) wide distribution under varying gap size.

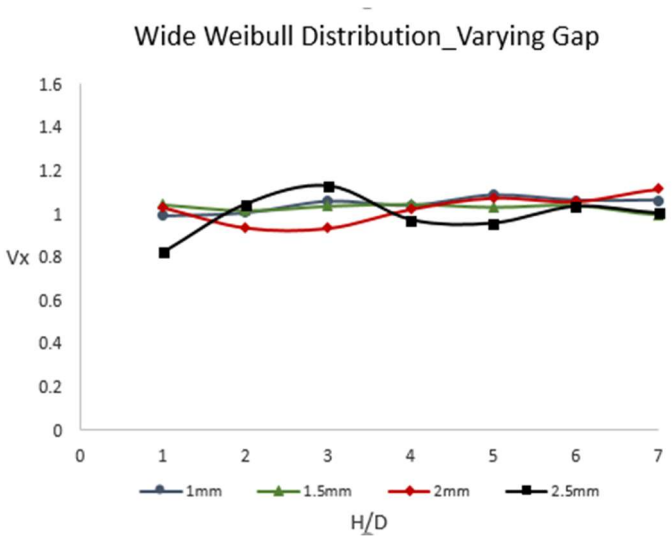

(c)

Figure 4.18 v_x distribution of particles with (a) narrow (b) uniform (c) wide distribution under varying gap size.

4.7. Parameter Sweep

In an expanded parameter space, the simulation time and the cost increase significantly. As described in Section 3.3, GNU parallel computing is introduced to remedy the computational cost. GNU parallel has shown great effectiveness in assigning simulation tasks. Few processes conducted in this work are compared in the course of the computational time cost in Table 4.1.

Table 4.1

Time cost comparison of different computing strategy.

Running type	Number of cases	Processor quantity	Time cost
Serial	625	1	3 d
Serial	10000	1	>24 h (terminated)
GNU parallel	10000	200	8.5 h

The first 625 cases cover all simulations from Section 4.2-4.5. These 625 cases were run in serial with manual adjustments, which takes around three days of computational time in total. However, after expanding the parameter space, it becomes an impossible mission to run all cases with manual changes. Instead, a serial algorithm is generated to assign all simulations to a single processor. The task was terminated by the cluster due to the exceeding of cut-off computing time. The time can be estimated based on the time cost for the first 625 cases, reaching 1.5 months. Besides, there barely exists a margin if some errors happen during the serial running, and the failure can be catastrophic.

The GNU parallel has shortened the overall simulation time to around 8.5 hours by simultaneously requesting more processors and activating processors. Not only the time cost is reduced, but more control of the task assignment also allows more margin to run all simulations with some easy-to-fix errors from either cluster or human factors.

4.7.1 Lattice-based Parameter Sweep

As described in Chapter 3, MFR is used to represent the quality of the spreading process. A frequency distribution chart for each lattice space is generated based on the calculated MFR, as shown in Figure 4.19. The first direct observation of convergence comes from the MFR distribution in each lattice space.

In Figure 4.19, all lattice space contains many simulations getting “MFR=0”. This is likely due to the selection of the gap size range and the particle size range. In other words, most of these “zero” cases are from simulations that have a gap size smaller or equal to the particle size.

In reality, such parameter setup is unrealistic and should be avoided. However, for uniform coverage of the parameter space, such a phenomenon is unavoidable. Scaling up

the gap size range will break the 2-time size matching between the gap and the diameter and further result in more inefficient spreading cases. To compromise the unrealistic spreading and inefficient spreading, the current parameter space is adopted.

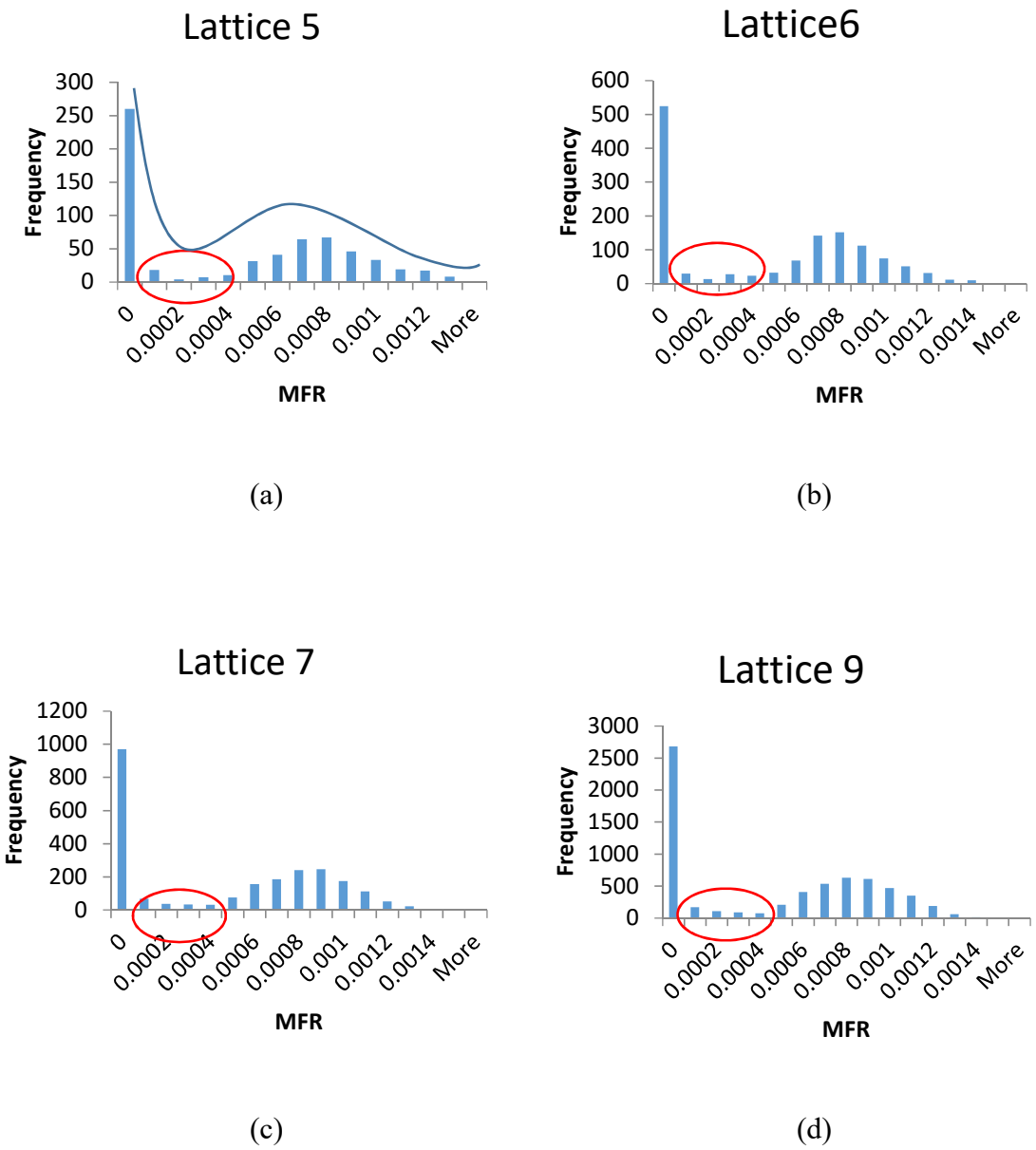

Figure 4.19 MFR Distribution in lattice space with grid of (a) 5(b) 6(c) 7(d) 9(e)10.

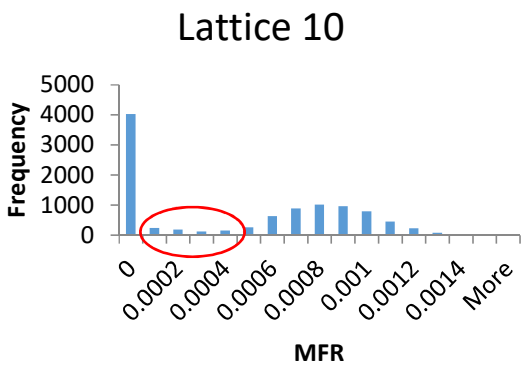

(e)

Figure 4.19 MFR Distribution in lattice space with grid of (a) 5(b) 6(c) 7(d) 9(e)10.

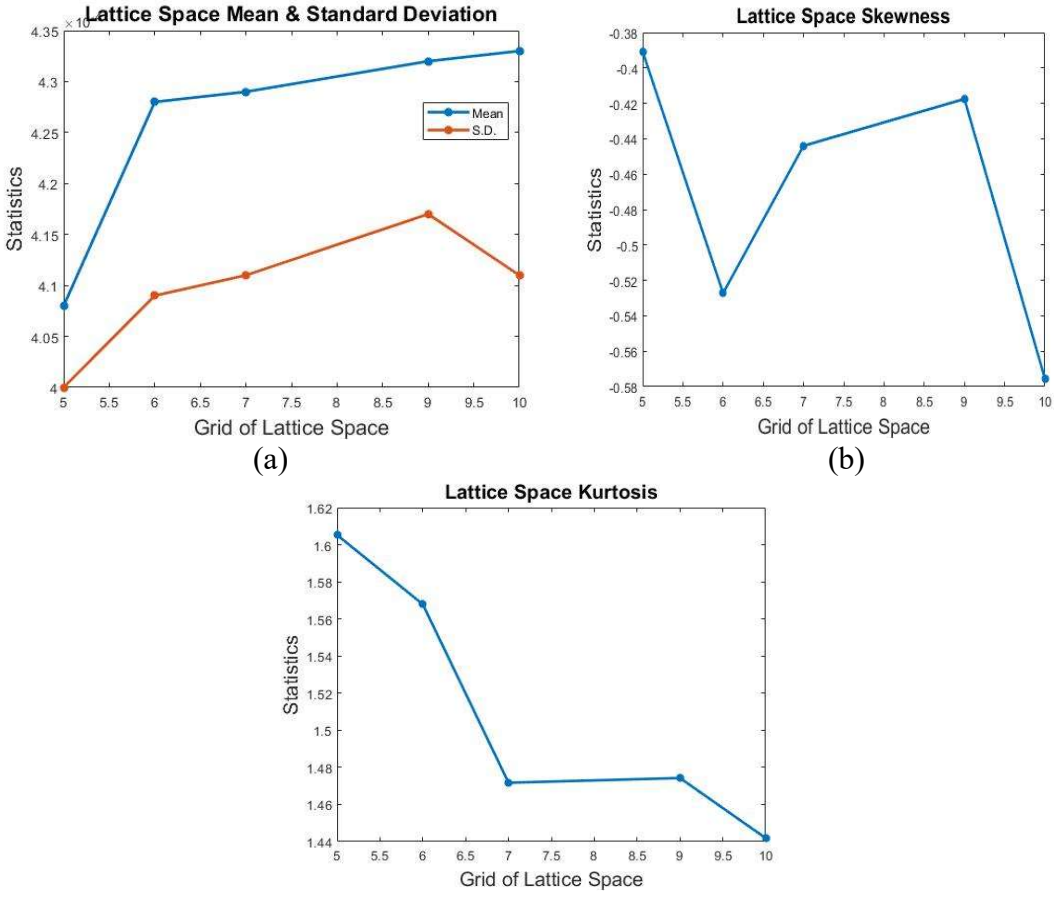

Figure 4.20 Statistics of MFR in lattice space (a) mean and standard deviation (b) skewness (c) kurtosis.

Some key features from the observation of MFR distribution are focused on. Firstly, despite the presence of the unrealistic spreading, the fitting trend in each lattice space is similar and consistent, which is a good sign of convergence and validation of the current parameter space. Besides, the valley area in Figure 4.19 shows some unneglectable difference between lattice 5 and lattice 9. However, the difference becomes less between lattice 9 and lattice 10, suggesting a sign of convergence.

To quantify the convergence of a lattice space, the variation of statistical measures is generated to describe the MFR distribution comprehensively, as illustrated in Figure 4.20. Once the relative change of one of the statistical measures falls into an acceptable range, the convergence is reached. By observing the statistical variation, lattice 10 is considered a convergence, with kurtosis first meeting the criterion. With that being said, the kurtosis is effective in checking the convergence of a lattice space in this work.

4.7.2. LDS Parameter Sweep

The same post-processing procedure is adopted in the LDS parameter sweep. The first observation of convergence comes from the MFR distribution, as shown in Figure 4.21. The featured valley and peak area in each LDS space are compared, seeking a sign of convergence. A guess of LDS convergence can be made in LDS 1600-2000 due to the slight differentiation between two continuous parameter spaces.

In the LDS parameter sweep, all four statistics are obtained by expanding the LDS parameter space, as presented in Figure 4.22. Observing the statistical variation for each LDS space, specifically the variation of standard deviation, LDS space with 1600 cases should be sufficient in describing the parameter space. Compared with the 10,000 cases

required in the lattice-based sweep, the LDS parameter sweep has greatly reduced the required number of simulations.

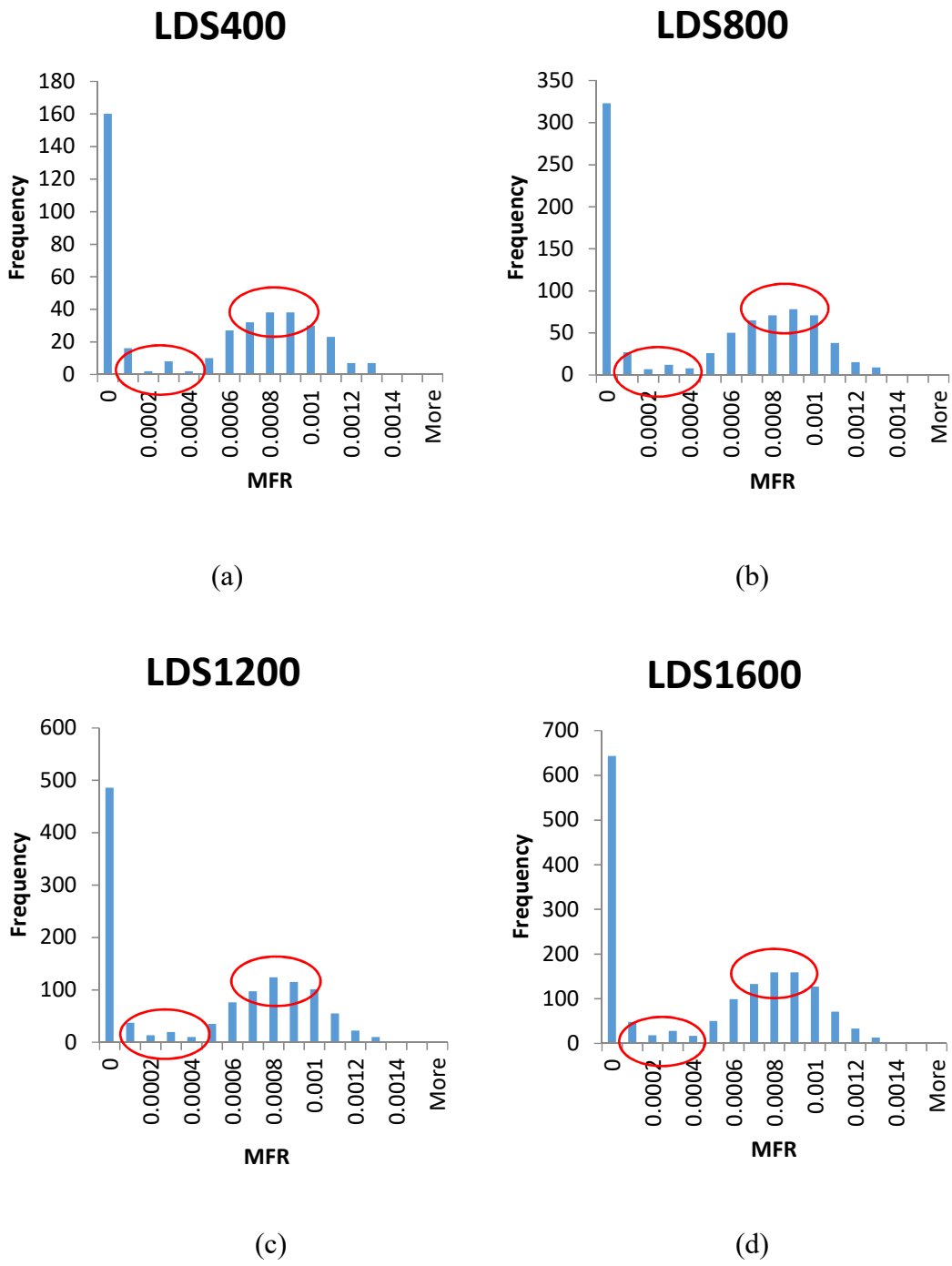

Figure 4.21 MFR distribution in LDS space of (a) 400 (b) 800 (c) 1200 (d) 1600 (e) 2000 (f) 2400.

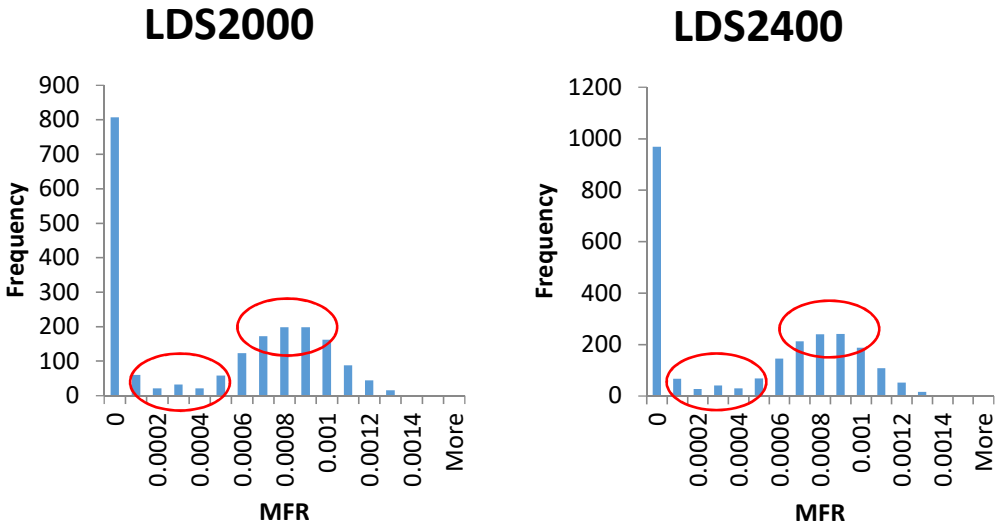

(e) (f)

Figure 4.21 MFR distribution in LDS space of (a) 400 (b) 800 (c) 1200 (d) 1600 (e) 2000 (f) 2400.

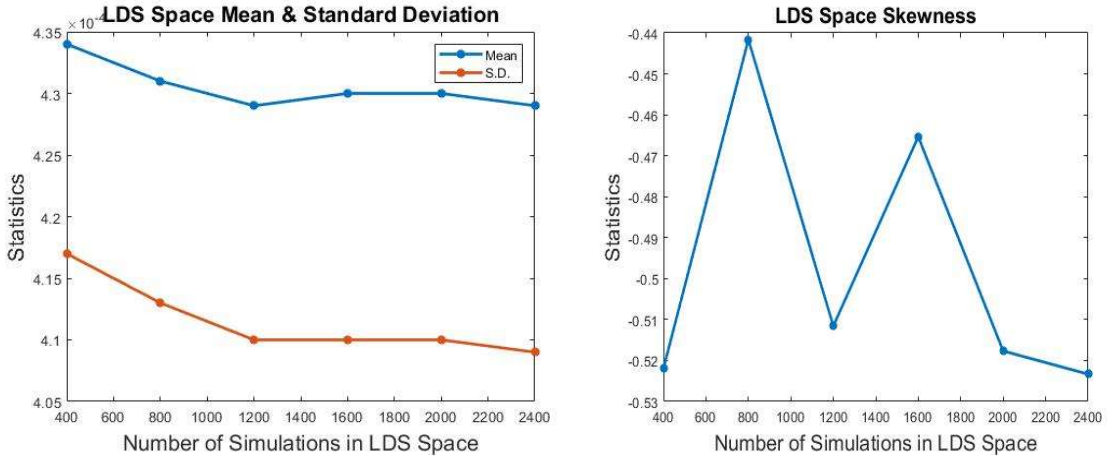

(a) (b)

Figure 4.22 Statistics of MFR in LDS Space (a) mean and standard deviation (b) skewness (c) kurtosis.

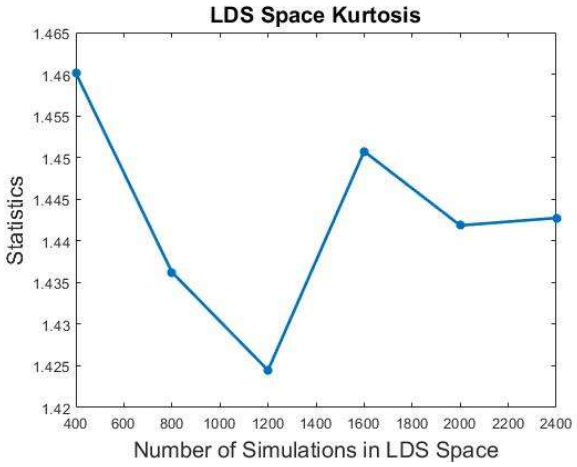

(c)

Figure 4.22 Statistics of MFR in LDS Space (a) mean and standard deviation (b) skewness (c) kurtosis.

5. Discussions and Conclusions

In this chapter, assumptions made for this work are validated with some previous relevant studies. In addition, by correlating other DEM simulation studies, all results presented in this work are discussed and compared.

5.1. Assumptions For Reducing Computational Cost

When a DEM simulation is designed, it is essential to balance the computational cost and accuracy. A few modeling assumptions are necessary to reduce the computational cost. One such assumption is regarding Young's Modulus. To use the real Young's Modulus in metallic material DEM, an extremely small timestep is required, which unfortunately results in an extremely long computational time (Kuo et al., 2002). The Young's Modulus can be the most important property of the material for describing the stiffness, and the normal elastic coefficient of the contact model is directly based on the Young's Modulus. As observed in a previous study that is about speeding up the DEM simulation (Lommen et al. 2014), the change of the modulus can directly lead to a change of the particle stiffness so that not only the interaction between particles but also the interaction between material and simulation box can be altered, which requires an extreme caution from DEM user.

However, such modulus reduction, or further, the normal elastic coefficient reduction has been found to be effective in increasing the time step size, and the simulation result is confirmed to be insensitive to such modification. (Han et al., 2019). Several studies with DEM simulations listed in Table 5.1 below use a lower Young's modulus lower than the actual Young's modulus.

Another sacrifice to be made for balancing the computational cost lies in the selection of the particle diameter. To be specific, in reality, the diameter of a stainless-steel particle is approximately around 0.045mm. However, in this work, the particle diameter has been scaled up. The reason for this scaling is that, before particles are inserted into the simulation box, they have to be firstly generated in an "insertion box" with a fixed volume. Smaller particles tend to fill the insertion box compactly with a larger number of particles, which leads to a longer simulation time (Tekeste, 2015).

Table 5.1

Young's Modulus assumptions for reducing the computational cost.

Assumption Type	Realistic Value	Reduced Value	Reference
Young's Modulus	0.7 GPa	70 MPa	Yuu et al., 1995
	2,004 MPa	0.2 MPa	Ghasemi et al., 2020
	55 GPa	55 MPa	Chen et al., 2017
	146 GPa	2 GPa	Han et al., 2019
Normal stiffness	40,000 N/m	1,000 N/m	Martins et al., 2013
	80,000 N/m	800 N/m	Kuwagi et al., 2000

In the previous study (Nan & Ghadiri, 2019), only a limited number of simulations may be enough to support the result, but such limited simulations are way too insufficient to support the parametric analysis. Thus, the particle diameter is scaled around 4-5 times as the real diameter, and the size distributions are based on this scaled diameter. The result suggests that the simulation time for each parameter setup is shortened to an acceptable range without losing much of potential particle behavior in the analysis with such a scale.

The scaling of particle property, such as size, is commonly done in DEM modeling studies for the consideration of computational cost. In Kawaguchi et al. (2000), the

particle size was scaled from 1.41mm to 3mm for balancing the computational cost. In some previous studies (Lee et al., 2018; Lommen et al., 2014), the mass of particles is scaled up, allowing a shorter time for particles' freefall behavior due to the gravity. These works suggested that scaling of the particle mass is a promising solution for efficiently reducing the simulation time.

5.2. Parametric Analysis

The influence of the gap size from this work can be generalized as follows. When the gap size is two times the average particle diameter, an optimum flow behavior can be produced. When the gap is too large for the particle diameter, an inefficient particle flow is generated, which is also observed as a "short-feed" effect (Nan & Ghadiri, 2019). They observe a similar critical gap size allowing particle spreading on the platform without empty patches in their work.

In a realistic particle spreading process, the gap size can be converted into a significant parameter of the printing process, namely, the layer thickness. In both polymer additive manufacturing and metallic additive manufacturing, the layer thickness is vital for generating a smooth flow and a higher-quality particle bed. Han et al. (2014) studied the effect of layer thickness on printed part quality. When the gap layer thickness is smaller than the average particle diameter, most particles tend to move with the blade and finally get pushed off the platform. This experimental observation is similar to the results in the current study. Another reason for the layer thickness being significant is that a thicker layer requires more concentrated energy to bond or melt the particles, which should also be considered in determining the upper limit of the layer thickness.

The influence of the particle size from this work can be concluded as follows. In general, a smaller particle size tends to produce a smoother velocity distribution contributing to a better particle flow performance. Such a result can match some of the previous works. For example, it was observed that too large particles tend to generate a so-called "short feed" effect that corresponds to cases of unrealistic spreading (Han et al., 2014). Additionally, as observed in Han et al. (2014), if the particle diameter is too small, there will be larger voids during the spreading. However, a similar result is not observed in the current work. A possible reason for this is the selection of the particle diameter and the contact model. The particle size has been scaled, and the particle cohesion is not considered in the contact model to save some computational cost, whereas a realistic particle size around $30\mu m$ is used in their work. Notice that, when the particle size is relatively small, the motion of the particle can not only depend on the gravity and contacting force but also depend on or even get dominated by the cohesion effect. Agglomeration is commonly observed in the behavior of small particles (Bai et al. (2015)). However, when cohesion between particles is not considered, similar behavior of smaller particles to this work was observed by Chen et al. (2017).

Another key parameter is friction. It is found that a higher quality of the spreading process can be obtained by lowering the friction between particles. Friction transfers the forces between particles providing particles with accelerating ability that makes particles move with the blade.

Higher friction is also found to reduce the particle spreading quality in other studies as well (Chen et al., 2017). The particle flow fluidity was found to decrease when increasing the friction coefficient between particles in their work. Such a phenomenon is

explained by the restriction of the relative motion between particles in the flow. They also report that the friction was found to influence the powder packing density on the printing platform. Particle-wall friction has not been considered in this thesis, which may also have some potential influence that needs to be considered in the future.

Blade speed has not been studied much in previous research. Among the limited studies, Nan et al. (2018) found that a lower blade speed can benefit the particle spreading by allowing particles enough time to go through the gap. This observation is similar to what is found in this thesis. Additionally, in their work, the blade motion was correlated with the gap size for explaining the shape change of the particle pile in front of the blade. Parteli et al. (2016) suggest that a faster spreading process creates looser particle packing due to the presence of larger voids, which is indirectly confirmed in this work as well.

Based on the effect of the large particles, some conclusions are drawn for the effect of particle size distribution. The previous analysis observed that lower friction and a slower blade can produce higher spreading quality. All parameters in simulations for the particle size distribution analysis are used with ideal values. Namely, the friction coefficient is 0.1, and the blade speed is 1.2m/s, to minimize the effect from other variables. The worst flow behavior comes from the 3mm case with a wide Weibull distribution and a 5mm gap. This is understandable because of the existence of 3.5mm and 4mm particles significantly affecting the flow behavior due to the relatively small gap size. Other than this extreme case, most of the results and analysis match well with the previous analysis with uniform particle diameters. For example, the 2:1 ratio between the gap size and the

particle size for optimal spreading still exists. With an optimal gap size, both mixed particles and uniform particles can produce a more ideal flow.

For small particles, both mixed particles and uniform particles can produce a smooth flow with an optimum gap. However, for larger particles, the performance of mixed particles with a narrow distribution is generally better than uniform particles, which brings out the powder quality effect considering the presence of narrower distribution in a higher quality powder. Based on the analysis of the uniform particle simulations, the observations of narrow distribution can be related to the existence of smaller particles. This is also noted by Lee et al. (2018). Further simulations can be conducted for a left-skewed distribution to investigate and quantify this effect.

5.3. Parameter Sweep

LDS based parameter sweep algorithm is found to be effective in reducing the number of DEM simulations without sacrificing the comprehensive description of the parameter space. Even though the parameter sweep is a common tool for optimizing a large multi-dimensional parameter space, it is rare to be applied in additive manufacturing or the DEM simulation. This parameter sweep algorithm has been applied in pedestrian dynamics studies involving many trajectories for analysis. The application of parameter sweep algorithms for additive manufacturing simulations in this work has been done for the first time and is a novel contribution.

Although it is hard to find some reference in a similar field, some similar studies applying the parameter sweep can be referred to draw some ideas on the performance of the sweep algorithm. A previous study (Chunduri et al., 2018) about optimizing pedestrian dynamics simulations by the parameter sweep compared lattice-based

parameter sweep and the LDS parameter sweep. They found that the LDS algorithm effectively reduced the number of simulations with similar coverage of the original parameter space. This observation is similar to the results of the current work. Specifically, the number of trajectories for their parameter space is reduced from the order of millions to around 30,000.

However, there is some difference between their work and this study regarding the statistical convergence measures. Specifically, in their work, both kurtosis and skewness were effective in checking convergence. However, in this thesis, probably due to the different parameter space selection, skewness is not as effective as kurtosis. This may indicate that the performance of statistics for checking convergence may depend on the specific parameter space and bring up the benefit of using multiple statistics to comprehensively describe the parameter space.

5.4. Conclusions

In this work, a parametric analysis is performed for the particle behavior during the particle spreading process in metallic additive manufacturing. Particle diameter, spreading gap size, printing blade speed, and inter-particle friction are cross-analyzed to optimize the particle flow smoothness. The primary conclusions of this research are listed below.

(1) To obtain a particle flow with higher quality, the particle diameter is the most dominant factor. Smaller particles tend to have an ideal velocity distribution. However, the performance of smaller particles depends on the gap size as well. When the gap size is two times the particle diameter, a more ideal flow behavior is observed. Gap sizes larger than two times the particle diameter lead to

inefficient spreading processes, and similarly smaller gap sizes relative to particle size lead to unrealistic spreading processes.

(2) Compared with the particle diameter and the gap size, the blade speed and inter-particle friction have less effect on the flow behavior. Blade speed affects particle spreading more than the friction. A lower blade speed tends to produce a smoother flow. In reality, reducing the blade speed can be a solution to improving manufacturing quality. However, a lower spreading speed corresponds to a longer manufacturing time.

(3) The inter-particle friction has the least effect on flow behavior. Higher friction can deteriorate the particle spreading by restricting the relative motion between particles, making particles move with the blade, creating an inefficient particle spreading.

(4) A narrow Weibull distribution, which is indicative of higher quality powder, leads to a better flow behavior. Specifically, smaller particles with a narrow distribution can produce a high-quality particle spreading. With such powder texture, an optimum gap, namely, twice as the mean particle size, improves the particle spreading quality.

(5) To reduce the computational cost of the parametric analysis, the lattice-based parameter sweep and the LDS parameter sweep are conducted in expanded parameter space. A computing tool called GNU parallel is applied to minimize the time cost for the massive simulation job and is shown to be highly effective. In lattice-based parameter space, nine intervals with ten grid values on each parameter range are sufficient to describe the 4-dimensional parameter space in

this work. Four statistical measures check the performance, and the kurtosis is effective in checking the convergence.

(6) LDS parameter sweep is more effective in reducing the number of simulations required to describe the parameter space. The data points for LDS sweep are generated using scrambled Halton sequence and scaled to fit the current parameter space. LDS parameter space converges at 2400 LDS simulations compared to 10,000 simulations needed for the lattice-based sweep.

6. Recommendations for Future Work

Considering some limitations existing in the current research, few recommendations relating to future work are listed based on all results of this thesis. By accordingly modifying the current methodology, it is feasible to perform a more realistic simulation which should provide a deeper understanding for the particle spreading procedure.

In current work, all DEM simulations focus on the first-layer spreading. In a realistic multi-layer particle spreading, i.e., repeating the spreading process layer by layer, the interaction of particles is no longer restricted between unbounded particles but also between the particle and the printed part. Sintered particles have various material properties resulting in a more complex spatial particle interaction, which can be an extension of the current work.

With the extraordinary ability of DEM, the bonding procedure can be simulated as well. The laser bonding energy and the laser scan rate were studied and found to influence the particle fusion in additive manufacturing (Han et al., 2019). Researchers have also studied the laser bonding procedure, including the aspects of heat transfer (Lee & Zhang, 2015). Also, the binder jetting process has been successfully simulated and investigated (Miao et al., 2019). Research along these lines is a promising extension to the current work.

One limitation of this work lies in the correlation between the experiment and the simulation. On the one hand, most of the parameters used in simulations are obtained from other papers. It is found in this work that material properties such as friction and particle diameter can influence the flow behavior. Therefore, experimentation will provide stronger support for the parametric analysis. The post-processing in this work

uses numerically defined parameters. However, it is feasible to evaluate the performance of the particle spreading by the experimentally measured surface roughness and packing density of the particle bed (Chen et al., 2020). The addition of experiments to validate the computational models can improve the understanding of flow behavior and printing quality.

From the numerical perspective, DEM provides the particle status with data intermittently, which means limited information when investigating the macroscopic flow behavior such as the continuous profile variation of the particle pile. Such intermittent particle status maybe lacks transient status. Plus, the complexity of DEM simulation comes from replicating a realistic particle spreading, which results in an unnecessary computational cost when the individual particle motion is not the focus of the study.

The purpose of DEM is to observe the macroscopic group behavior by defining the interaction between individuals. This is similar to the idea of Agent-Based Modeling (ABM) (Wilensky et al., 2015). In general, ABM has been greatly used in natural science and social science. The power of ABM lies in reducing the complexity of the simulation system by providing a simplified simulation. Depending on the interaction model, ABM has been used extensively in pedestrian dynamics (Chen et al., 2015; Pan et al., 2007). Besides, ABM also provides continuous tracking of the flow, which means a potential solution to continuous monitoring of the particle flow compared with DEM.

The same particle spreading procedure has been replicated in an ABM software called Netlogo (Wilensky., 1999) with the same contact model as a preliminary extension of the current model. The greatest benefit lies in the reduction of the complexity in the DEM

simulation system. Since the ABM has not yet been used for studying particle dynamics in additive manufacturing, it will be a promising and novel extension of current work.

Another extension of this work exists in the study of particle size distribution. In reality, it is extremely hard to find metallic powder with a uniform size distribution. The primary objective of all uniform particle size distribution in this work is to understand the general flow behavior when varying the particle size. Additionally, it was found in this work that mixed particle powder with a Weibull distribution can influence the flow behavior. The two Weibull parameters can be varied to describe the various particle size distribution, resulting in a further expansion of 4-dimensional parameter space to 6-dimensions. The large parameter space can be adequately studied using the LDS parameter sweep as demonstrated in this thesis.

REFERENCES

Abbasfard, H., Evans, G., & Moreno-Atanasio, R. (2016). Effect of van der Waals force cut-off distance on adhesive collision parameters in DEM simulation. Powder Technology, 299, 9-18.

Ahn, S., Montero, M., Odell, D., Roundy, S., & Wright, P. K. (2002). Anisotropic material properties of fused deposition modeling ABS. Rapid Prototyping Journal, 8(4), 248-257.

Ahrens, J., Geveci, B., & Law, C. (2005). ParaView: An end-user tool for large-data visualization.

Averardi, A., Cola, C., Zeltmann, S. E., & Gupta, N. (2020). Effect of particle size distribution on the packing of powder beds: A critical discussion relevant to additive manufacturing. Materials Today Communications, 24, 100964.

Azevedo, N. M., & Lemos, J. V. (2006). Hybrid discrete element/finite element method for fracture analysis. Computer Methods in Applied Mechanics and Engineering, 195(33-36), 4579-4593.

Bai, Y., Wagner, G., & Williams, C. B. (2015). Effect of bimodal powder mixture on powder packing density and sintered density in binder jetting of metals. In 2015 Annual International Solid Freeform Fabrication Symposium (Vol. 62, pp. 758-771).

Beecroft, M. (2016). 3D printing of weft knitted textile based structures by selective laser sintering of nylon powder. IOP Conference Series. Materials Science and Engineering, 137(1), 012017.

Braaten, E., & Weller, G. (1979). An improved low-discrepancy sequence for multidimensional quasi-monte carlo integration. Journal of Computational Physics, 33(2), 249-258.

Campbell, I., Bourell, D., & Gibson, I. (2012). Additive manufacturing: Rapid prototyping comes of age. Rapid Prototyping Journal, 18(4), 255-258.

Chen, F., Wang, Z., & Zhu, Y. (2015). Agent-based continuous-space particle pedestrian model. Proceedings of the Institution of Civil Engineers. Transport, 168(4), 336-345.

Chen, H., Wei, Q., Wen, S., Li, Z., & Shi, Y. (2017). Flow behavior of powder particles in layering process of selective laser melting: Numerical modeling and experimental verification based on discrete element method. International Journal of Machine Tools & Manufacture, 123, 146-159.

Chen, H., Xiao, Y. G., Liu, Y. L., & Shi, Y. S. (2017). Effect of young's modulus on DEM results regarding transverse mixing of particles within a rotating drum. Powder Technology, 318, 507-517.

Chen, H., Chen, Y., Liu, Y., Wei, Q., Shi, Y., & Yan, W. (2020). Packing quality of powder layer during counter-rolling-type powder spreading process in additive manufacturing. International Journal of Machine Tools & Manufacture, 153, 103553.

Chen, X., & Elliott, J. A. (2020). On the scaling law of JKR contact model for coarse-grained cohesive particles. Chemical Engineering Science, 227, 115906.

Camones, L. A. M., Vargas, E. d. A., de Figueiredo, R. P., & Velloso, R. Q. (2013). Application of the discrete element method for modeling of rock crack propagation and coalescence in the step-path failure mechanism. Engineering Geology, 153, 80-94.

Cheong, Y. S., Zhao, A., Ahmadian, H., Bi, W., & Shen, R. (2014). Discharge Analysis of an Industrial Batch Rotating Drum. In Particle Science and Engineering (pp. 122-125).

Chunduri, S., Ghaffari, M., Sadeghi Lahijani, M., Srinivasan, A., & Namilae, S. (2018). Parallel low discrepancy parameter sweep for public health policy. Paper presented at the 291-300.

Cundall, P. A., & Strack, O. D. L. (1980). Discussion: a discrete numerical model for granular assemblies. Geotechnique, 30(3), 331-336.

Deng, X. L., & Davé, R. N. (2013). Dynamic simulation of particle packing influenced by size, aspect ratio and surface energy. Granular Matter, 15(4), 401-415.

Di Renzo, A., & Di Maio, F. P. (2004). Comparison of contact-force models for the simulation of collisions in DEM-based granular flow codes. Chemical Engineering Science, 59(3), 525-541.

Drummer, D., Cifuentes‐Cuéllar, S., & Rietzel, D. (2012). Suitability of PLA/TCP for fused deposition modeling. Rapid Prototyping Journal, 18(6), 500-507.

Fang, Z., Patterson, B. R., & Turner Jr, M. E. (1993). Modeling particle size distributions by the weibull distribution function. Materials Characterization, 31(3), 177-182.

Froes, F. H., & Dutta, B. (2014). The additive manufacturing (AM) of titanium alloys. Paper presented at the , 1019 19-25.

Gan, J. Q., Yu, A. B., & Zhou, Z. Y. (2016). DEM simulation on the packing of fine ellipsoids. Chemical Engineering Science, 156, 64-76.

Ghasemi, A. R., Razi, E., & Banisi, S. (2020). Determining a lower boundary of elasticity modulus used in the discrete element method (DEM) in simulation of tumbling mills. Advanced Powder Technology : The International Journal of the Society of Powder Technology, Japan, 31(4), 1365-1371.

Grayson, W. L., Fröhlich, M., Yeager, K., Bhumiratana, S., Chan, M. E., Cannizzaro, C., . . . Vunjak-Novakovic, G. (2010). Engineering anatomically shaped human bone grafts. Proceedings of the National Academy of Sciences - PNAS, 107(8), 3299-3304.

Haeri, S. (2017). Optimisation of blade type spreaders for powder bed preparation in additive manufacturing using DEM simulations. Powder Technology, 321, 94-104.

Haeri, S., Wang, Y., Ghita, O., & Sun, J. (2017). Discrete element simulation and experimental study of powder spreading process in additive manufacturing. Powder Technology, 306, 45-54.

Han, Q., Gu, H., & Setchi, R. (2019). Discrete element simulation of powder layer thickness in laser additive manufacturing. Powder Technology, 352, 91-102.

Harun, W. S. W., Kamariah, M. S. I. N., Muhamad, N., Ghani, S. A. C., Ahmad, F., & Mohamed, Z. (2018). A review of powder additive manufacturing processes for metallic biomaterials. Powder Technology, 327, 128-151.

Helbing, D., & Molnár, P. (1995). Social force model for pedestrian dynamics. Physical Review. E, Statistical Physics, Plasmas, Fluids, and Related Interdisciplinary Topics, 51(5), 4282-4286.

Hermez, M., Jawad, B., Liu, L., & Kheirallah, M. (2019). Subtractive/Additive rapid prototyping of a curve spacer for centrifugal pump impeller: Design, manufacturing, and simulation analysis.

Jiang, M. J., Liu, J., Sun, C., & Chen, H. (2015). DEM analyses of shear behaviour of rock joints by a novel bond contact model. Paper presented at the , 26(1) 12021.

Johnson, K. L., Kendall, K., & Roberts, A. (1971). Surface energy and the contact of elastic solids. Proceedings of the royal society of London. A. mathematical and physical sciences, 324(1558), 301-313.

Karapatis, N. P., Egger, G., Gygax, P. E., & Glardon, R. (1999). Optimization of powder layer density in selective laser sintering. In 1999 International Solid Freeform Fabrication Symposium.

Kawaguchi, T., Sakamoto, M., Tanaka, T., & Tsuji, Y. (2000). Quasi-three-dimensional numerical simulation of spouted beds in cylinder. Powder Technology, 109(1), 3-12.

Kiss, T., Greenwell, P., Heindl, H., Terstyanszky, G., & Weingarten, N. (2010). Parameter sweep workflows for modelling carbohydrate recognition. Journal of Grid Computing, 8(4), 587-601.

Kloss, C., Goniva, C., Hager, A., Amberger, S., & Pirker, S. (2012). Models, algorithms and validation for opensource DEM and CFD-DEM. Progress in Computational Fluid Dynamics, 12(2-3), 140-152.

Kocis, L., & Whiten, W. (1997). Computational investigations of low-discrepancy sequences. ACM Transactions on Mathematical Software (TOMS), 23(2), 266-294.

Kolenikov, S. (2012). Scrambled halton sequences in mata. The Stata Journal, 12(1), 29-44.

Kruggel-Emden, H., Wirtz, S., Simsek, E., & Scherer, V. (2006). Modeling of granular flow and combined heat transfer in hoppers by the discrete element method (DEM).

Kuo, H. P., Knight, P. C., Parker, D. J., Tsuji, Y., Adams, M. J., & Seville, J. P. K. (2002). The influence of DEM simulation parameters on the particle behaviour in a V-mixer. Chemical Engineering Science, 57(17), 3621-3638.

Kuwagi, K., Mikami, T., & Horio, M. (2000). Numerical simulation of metallic solid bridging particles in a fluidized bed at high temperature. Powder Technology, 109(1), 27-40.

Langston, P. A., Tüzün, U., & Heyes, D. M. (1994). Continuous potential discrete particle simulations of stress and velocity fields in hoppers: Transition from fluid to granular flow. Chemical Engineering Science, 49(8), 1259-1275.

Lee, Y. S., Nandwana, P., Zhang, W., & Oak Ridge National Lab. (ORNL), Oak Ridge, TN (United States). (2018). Dynamic simulation of powder packing structure for powder bed additive manufacturing. International Journal of Advanced Manufacturing Technology, 96(1-4), 1507-1520.

Lee, Y. S., & Zhang, W. (2015, August). Mesoscopic simulation of heat transfer and fluid flow in laser powder bed additive manufacturing. In International Solid Free Form Fabrication Symposium, Austin (pp. 1154-1165).

Liu, H., Li, J., & Wang, Q. (2017). Simulation of gas–solid flow characteristics in a circulating fluidized bed based on a computational particle fluid dynamics model. Powder Technology, 321, 132-142.

Lu, K., & Reynolds, W. T. (2008). 3DP process for fine mesh structure printing. Powder Technology, 187(1), 11-18.

Luecke, W. E., & Slotwinski, J. A. (2014). Mechanical properties of austenitic stainless steel made by additive manufacturing. Journal of Research of the National Institute of Standards and Technology, 119(1), 398-418.

Lommen, S., Schott, D., & Lodewijks, G. (2014). DEM speedup: Stiffness effects on behavior of bulk material. Particuology, 12(1), 107-112.

Manfredi, D., Calignano, F., Ambrosio, E. P., Krishnan, M., Canali, R., Biamino, S., . . . Badini, C. (2013). Direct metal laser sintering: An additive manufacturing technology ready to produce lightweight structural parts for robotic applications. Metallurgia Italiana, 105(10), 15-24.

Martins, S., Li, W., Radziszewski, P., Faucher, A., & Makni, S. (2013). Experimental and simulated instrumented ball in a tumbling mill—A comparison. Minerals Engineering, 43-44, 79-84.

Miao, G., Du, W., Pei, Z., & Ma, C. (2019). Binder jetting additive manufacturing of ceramics: analytical and numerical models for powder spreading process. In ASME 2019 14th International Manufacturing Science and Engineering Conference. American Society of Mechanical Engineers Digital Collection.

Mindlin, R.D. (1949). “Compliance of elastic bodies in contact”. In: Journal of Applied Mechanics, pp. 259–268.

Mohamed, O. A., Masood, S. H., & Bhowmik, J. L. (2016). Analytical modelling and optimization of the temperature-dependent dynamic mechanical properties of fused deposition fabricated parts made of PC-ABS. Materials, 9(11), 895.

Moreno Madrid, A. P., Vrech, S. M., Sanchez, M. A., & Rodriguez, A. P. (2019). Advances in additive manufacturing for bone tissue engineering scaffolds. Materials Science and Engineering: C, 100, 631-644.

Morokoff, W. J., & Caflisch, R. E. (1994). Quasi-random sequences and their discrepancies. SIAM Journal on Scientific Computing, 15(6), 1251-1279.

Munjiza, A., Owen, D. R. J., & Bicanic, N. (1995). A combined finite‐discrete element method in transient dynamics of fracturing solids. Engineering Computations, 12(2), 145-174.

Nan, W., Pasha, M., Bonakdar, T., Lopez, A., Zafar, U., Nadimi, S., & Ghadiri, M. (2018). Jamming during particle spreading in additive manufacturing. Powder Technology, 338, 253-262.

Nan, W., & Ghadiri, M. (2019). Numerical simulation of powder flow during spreading in additive manufacturing. Powder Technology, 342, 801-807.

Nandy, J., Sarangi, H., & Sahoo, S. (2019). A review on direct metal laser sintering: Process features and microstructure modeling. Lasers in Manufacturing and Materials Processing, 6(3), 280-316.

Pan, X., Han, C. S., Dauber, K., & Law, K. H. (2007). A multi-agent based framework for the simulation of human and social behaviors during emergency evacuations. AI & Society, 22(2), 113-132.

Pantaleev, S., Yordanova, S., Janda, A., Marigo, M., & Ooi, J. Y. (2017). An experimentally validated DEM study of powder mixing in a paddle blade mixer. Powder Technology, 311, 287-302.

Parteli, E. J. R., & Pöschel, T. (2016). Particle-based simulation of powder application in additive manufacturing. Powder Technology, 288, 96-102.

Patterson, A. E., Messimer, S. L., & Farrington, P. A. (2017). Overhanging features and the SLM/DMLS residual stresses problem: Review and future research need. Technologies (Basel), 5(2), 15.

Peng, B. (2014). Discrete element method (DEM) contact models applied to pavement simulation (Doctoral dissertation, Virginia Tech).

Plimpton, S. (1995). Fast parallel algorithms for short-range molecular dynamics. Journal of Computational Physics, 117(1), 1-19.

Rapaport, D. (2004). The art of molecular dynamics simulation (2nd ed.). Cambridge University Press.

Rubio del Solar, M., Boton-Fernandez, M., & Diaz Herrero, G. (2015). Energetic island design optimization. A case study using sweep parameter search and variable neighborhood search techniques. Paper presented at the , 2015-(June) 3108-3113.

Schmid, W. C., & Uhl, A. (2001). Techniques for parallel quasi-monte carlo integration with digital sequences and associated problems. Mathematics and Computers in Simulation, 55(1), 249-257.

Schoinochoritis, B., Chantzis, D., & Salonitis, K. (2016;2017;). Simulation of metallic powder bed additive manufacturing processes with the finite element method: A

critical review. Proceedings of the Institution of Mechanical Engineers. Part B, Journal of Engineering Manufacture, 231(1), 96-117.

Seidel, A., Saha, S., Maiwald, T., Moritz, J., Polenz, S., Marquardt, A., . . . Leyens, C. (2019). Intrinsic heat treatment within additive manufacturing of gamma titanium aluminide space hardware. Jom (1989), 71(4), 1513-1519.

Shmulevich, I. (2010). State of the art modeling of soil–tillage interaction using discrete element method. Soil & Tillage Research, 111(1), 41-53.

Simchi, A., Petzoldt, F., & Pohl, H. (2003). On the development of direct metal laser sintering for rapid tooling. Journal of Materials Processing Technology, 141(3), 319-328.

Simchi, A. (2006). Direct laser sintering of metal powders: Mechanism, kinetics and microstructural features. Materials Science & Engineering. A, Structural Materials : Properties, Microstructure and Processing, 428(1-2), 148-158.

Sinico, M., Witvrouw, A., & Dewulf, W. (2019). Influence of the particle size distribution on surface quality of Maraging 300 parts produced by Laser Powder Bed Fusion. In Proceedings of the Special Interest Group meeting on Advancing Precision in Additive Manufacturing (pp. 31-34). euspen.

Spierings, A. B., Herres, N., & Levy, G. (2011). Influence of the particle size distribution on surface quality and mechanical properties in AM steel parts. Rapid Prototyping Journal, 17(3), 195-202.

Srinivasan, A. (2002). Parallel and distributed computing issues in pricing financial derivatives through quasi monte carlo. Paper presented at the 6 pp-123.

Strano, G., Hao, L., Everson, R. M., & Evans, K. E. (2012;2013;). A new approach to the design and optimisation of support structures in additive manufacturing. International Journal of Advanced Manufacturing Technology, 66(9-12), 1247-1254.

Tan, J. H. K., Sing, S. L., & Yeong, W. Y. (2019;2020;). Microstructure modelling for metallic additive manufacturing: A review. Virtual and Physical Prototyping, 15(1), 1-19.

Tange, O. (2011). Gnu parallel-the command-line power tool.; login: The USENIX Magazine, 36 (1): 42–47.

Vayre, B., Vignat, F., & Villeneuve, F. (2012). Metallic additive manufacturing: State-of-the-art review and prospects. Mechanics & Industry: An International Journal on Mechanical Sciences and Engineering Applications, 13(2), 89-96.

Tekeste, M. (2015). Discrete Element Modelling (DEM) For Earthmoving Equipment Design and Analysis: Opportunities and Challenges.

Tepylo, N., Huang, X., & Patnaik, P. C. (2019). Laser‐Based additive manufacturing technologies for aerospace applications. Advanced Engineering Materials, 21(11), 1900617-n/a.

Tuffin, B. (1996). On the use of low discrepancy sequences in Monte Carlo methods. Rennes, France: IRISA.

Wąs, J., Gudowski, B., & Matuszyk, P. J. (2006). Social distances model of pedestrian dynamics. Paper presented at the , 4173 492-501.

Watson, J. K., & Taminger, K. M. B. (2018;2015;). A decision-support model for selecting additive manufacturing versus subtractive manufacturing based on energy consumption. Journal of Cleaner Production, 176, 1316-1322.

Wilensky, U. (1999). Center for connected learning and computer-based modeling. In NetLogo. Northwestern University.

Wilensky, U., Rand, W., & JSTOR Collection. (2015). An introduction to agent-based modeling: Modeling natural, social, and engineered complex systems with NetLogo. Cambridge, Massachusetts: MIT Press.

Xiang, Z., Yin, M., Deng, Z., Mei, X., & Yin, G. (2016). Simulation of forming process of powder bed for additive manufacturing. Journal of Manufacturing Science and Engineering, 138(8).

Yadroitsev, I., Thivillon, L., Bertrand, P., & Smurov, I. (2007). Strategy of manufacturing components with designed internal structure by selective laser melting of metallic powder. Applied Surface Science, 254(4), 980-983.

Yamane, K. (2004). Discrete-element method application to mixing and segregation model in industrial blending system. Journal of Materials Research, 19(2), 623-627.

Yang, C., Gao, W., Liu, N., & Song, C. (2015). Low-discrepancy sequence initialized particle swarm optimization algorithm with high-order nonlinear time-varying inertia weight. Applied Soft Computing, 29, 386-394.

Yuan, S., Shen, F., Chua, C. K., & Zhou, K. (2019). Polymeric composites for powder-based additive manufacturing: Materials and applications. Progress in Polymer Science, 91, 141-168.

Yuu, S., Abe, T., Saitoh, T., & Umekage, T. (1995). Three-dimensional numerical simulation of the motion of particles discharging from a rectangular hopper using distinct element method and comparison with experimental data (effects of time

steps and material properties). Advanced Powder Technology : The International Journal of the Society of Powder Technology, Japan, 6(4), 259-269.

Zhang, Y., Wu, L., Guo, X., Kane, S., Deng, Y., Jung, Y., . . . Zhang, J. (2017;2018;). Additive manufacturing of metallic materials: A review. Journal of Materials Engineering and Performance, 27(1), 1-13.

Zhu, H. H., Lu, L., & Fuh, J. Y. H. (2003). Development and characterisation of direct laser sintering cu-based metal powder. Journal of Materials Processing Technology, 140(1-3), 314-317.

Ziegelmeier, S., Christou, P., Wöllecke, F., Tuck, C., Goodridge, R., Hague, R., Wintermantel, E. (2015). An experimental study into the effects of bulk and flow behaviour of laser sintering polymer powders on resulting part properties. Journal of Materials Processing Technology, 215(1), 239-250.

Zobeck, T., Gill, T., & Popham, T. (1999). A two-parameter weibull function to describe airborne dust particle size distributions. Earth Surface Processes and Landforms, 24(10), 943-955.

APPENDIX A – Parametric analysis post-processing algorithm

```
Program postprocessing
Implicit none

!This Algorithm is for calculating the average velocity distribution from the
!LIGGGHTS output file
!The algorithm is on the basis of Fortran 90
!All vriable values are defined by current simulation setup

real, allocatable      ::data(:,:) !Read particle status from LIGGGHTS outputs
integer                ::i, N, j, istep, layer
real                   ::D, gap, H,F, vxsum, num, vx, depth, Xlow, Xhigh, blade
num = 0
vxsum = 0

depth=0.001 !Determine the layer thickness for post-processing

F=0.1          !Input the friction
D=0.003     !Input the particle diameter
gap=0.005    !Input the gap
blade=1.2     !Input the blade speed

open(30, file= 'liggghts_output.txt')          !Define the input file for post-processing
open(31,file='postprocessing.txt')             !Define the output file for post-processing

read(30,*) N  ! Read the number of particles from the LIGGGHTS output
allocate(data(N,7))
do i=1,N
     read(30,*) (data(i,j),j=1,7) !Particle status in a matrix format for processing
enddo

Xlow =0.015+ blade * 0.00001 * 2000 * 5
Xhigh = Xlow + 6*D  !Define the post-processing area

do layer=1,12              !External loop for each layer with relative height
      do i=1,N             !Internal loop for calculating the average velocity
      H=gap + layer * D * 0.5
    !If particles fall in the post processing area
    if (data(i,2) >= Xlow .AND. data(i,2) <= Xhigh .AND. #
    data(i,4) >=(H-depth) .AND. data(i,4) <= (H+depth)) then
      num= num + 1 ! Calculate the particle number
      vxsum=vxsum+data(i,5)   !Calculate total x-velocity
      endif
      enddo
      vx=vxsum/num   !Calculate the average x-velocity
```

```
        write(31,*) vx  !Output vx distribution layer by layer
        num=0 !Initialize for next external loop
        vxsum=0
        vx=0
enddo

close(30)
close(31)

end program postprocessing
```

APPENDIX B – PBS script for GNU parallel

```
##This Bash code is for submitting a GNU parallel job to a cluster. The example script is for running 200 sequential tasks in GNU parallel
#!/bin/bash

#PBS -l walltime=02:00:00       #Set cut-off computing time
#PBS -l nodes=10:ppn=36         #Request a number of processors
#PBS -N jobname
#PBS -n
#PBS -q shortq
#PBS -m aeb
#PBS -M example@xxx.edu
#PBS -j oe
#PBS -d /scratch/target_directory


module load gcc/6.1.0
module load intel/mpi/64/2017/5.239
module load intel/compiler/64/2017/17.0.5
WORKING_DIR=/scratch/ target_directory


cd ${WORKING_DIR}

seq 1 200 | parallel -j 0 --sshloginfile $PBS_NODEFILE "cd ${WORKING_DIR}; ./run {} "
```